International Journal of Fracture, Vol. 18, No. 2 February 1982

The Hague, The Netherlands

The distribution of the elastic strain-energy density at the crack tip for fracture modes I and II

P.S. THEOCARIS and G. PAPADOPOULOS

Department of Theoretical and Applied Mechanics, The National Technical University of Athens 5, K. Zographou Street Zographou, Athens 624, Greece

(Received January 1, 1980; in revised form March 1, 1981)

ABSTRACT

The study of the distribution of the elastic-strain energy density at the tip of a crack presents a special interest for the understanding of the mechanism of fracture. In this investigation an exhaustive theoretical analysis of the distribution of the elastic-strain energy density at the tip of a crack for cracks in isotropic elastic media deformed under modes I and II was developed.

This study was complemented by an experimental solution of this type of problem, based on the method of reflected caustics. According to this method the distribution of the elastic-strain energy density was evaluated along a circular closed curve, defining the singular core around the crack-tip, which was dominated by the singularity at the crack tip and whose diameter is very small, not exceeding a few millimeters. In this way the situation at the crack-tip singularity was directly depicted on the energy density distribution. Interesting results concerning the factors influencing the mode of the strain energy distribution around the crack and the type of the crack path were derived.

List of Symbols

W = elastic strain energy.
dW/dV = elastic strain energy density.
G, E = shear and elastic modulus of the material respectively.
ν = Poisson's ratio.
$\sigma_{xx}, \sigma_{yy}, \tau_{xy}$ = crack tip stresses referred to Cartesian coordinate system.
σ_1, σ_2 = principal stresses at crack tip.
$\kappa_1 = (1-\nu)/(1+\nu)$ for plane stress.
$\kappa_2 = 1-2\nu$ for plane strain.
$\Phi(z), \Omega(z)$ = complex-stress functions of Muskhelishvili.
α = crack length.
k = ratio of stresses at infinity.
K_I, K_{II} = stress intensity factors for Modes I and II of loading, respectively.
r, ϑ = polar coordinate system centered at crack tip.
ω = angle of inclination of the crack.
μ = ratio of stress intensity factors $K_{II}/K_I = \tan\omega$ for uniaxial tension.
σ = stress applied at infinity along the transverse boundaries of the plate.
$\lambda = \sigma(1-k)\cos 2\omega$.
$X'_{r,f}, Y'_{r,f}$ = parametric equations of the reflected caustics referred to the Cartesian system $0'x'y'$ on the reference screen: (r) reflected caustics from rear face of the specimen and (f) reflected caustics from the front face of the specimen.
r_0 = radius of the generatrix curve on the specimen around the crack tip (initial curve).
$c_{r,f}$ = optical constants of the material for reflections from the rear and front faces of the specimen respectively.
λ_m = magnification ratio of the optical set-up.
z_0 = distance between the reference-screen and the middle plane of the specimen.
z_i = distance between the focus of the light beam and the middle plane of the specimen.
d = thickness of specimen.

$\epsilon = 2$ for the reflected caustics from the rear face of the specimen and 1 for the reflected caustics from the front face of the specimen.

$C_{r,f} = \epsilon z_0 \, d c_{r,f}/(2\pi)^{1/2}$

D_T^{max}, D_L^{max} = the maximum transverse and longitudinal diameters of the caustics respectively.

$\delta_T^{max}, \delta_L^{max}$ = the correction factors for D_T^{max} and D_L^{max} respectively.

$$f = (2\pi)^{-1/2} \left(\frac{3}{2} \frac{C_{r,f}}{\lambda_m}\right)^{-1/5}$$

E_1, E_2 = the areas of the upper and lower parts of the energy-density lobe respectively.

$E = E_1 + E_2$.

ϑ_{min} = the position of the minimum elastic-strain energy. Direction of crack propagation.

x_i, y_i = the coordinates of the propagating cracks tip O_i.

β = the projection of each propagation step on the transverse Ox-axis.

1. Introduction

An extensive theoretical study of the concept of the elastic-strain energy density was made by Sih in a series of papers [1 to 4]. Riedmüller [5] has determined experimentally the distribution of the energy density at the neighbourhood of a crack tip for cracks submitted to modes I and II of deformation, by applying classical photoelasticity and interferometry. These experimental methods are very convenient for classical whole-field elasticity problems. However, they lose their potentialities and accuracy when applied to singular stress fields, since they necessitate extrapolation of data far away of the singularity in order to evaluate the singular stress field. These inconveniences were removed by using the method of caustics, which gathers information from the close vicinity of the singularity, where the stress field is completely dominated by it [6, 7].

By applying the method of reflected caustics the distribution of the elastic strain-energy density (SED) along the initial curve of the caustic can be readily evaluated. The shape of this curve for isotropic and optically inert materials is always a circle, whose center lies at the close vicinity of the crack tip [8]. Thus, the elastic-strain energy density may be evaluated along the boundary of the singular core which is the circumference of this circle and its integral gives the total elastic-strain energy at the crack tip.

Various criteria have been introduced for the description of mode of propagation of a crack submitted to a combined mode I and II in-plane deformations. The most interesting criteria are the *maximum-stress criterion*, proposed by Erdogan and Sih [9], the *minimum strain-energy-density criterion*, proposed by Sih [1, 4, 10], and the *maximum-energy-release rate criterion*, proposed again by Erdogan and Sih [9].

According to the first criterion the crack is propagating at a direction normal to the direction of maximum tangential stress. The minimum strain-energy density criterion postulates that the crack propagates along the direction of minimum elastic-strain-energy density, whereas the maximum-energy-release rate criterion represents a generalization of Griffith's original energy-release-rate concept [11, 12]. According to this criterion the crack propagates along the maximum released strain energy.

In this paper the criterion of minimum strain-energy density (MESED) was studied. A detailed analysis of the distribution of the elastic-strain-energy density in combination with the optical method of reflected caustics was undertaken. From the evaluation of the distribution of the elastic-strain-energy density around the crack tip and along the small circle surrounding the crack tip and representing the generatrix curve of the caustic (*initial curve*) the total strain-energy was evaluated in terms of the characteristics of the caustics. Finally, the path of a propagating crack was established analytically, based on the same theory and compared with experimental results from propagating cracks in polymers.

2. The elastic strain energy

The elastic-strain energy dW stored in a parallelopiped of volume dV for plane-stress conditions dominating at the strained plate is expressed by [4]:

$$\frac{dW}{dV} = \frac{1}{8G}\left[\frac{(1-\nu)}{(1+\nu)}(\sigma_{xx}+\sigma_{yy})^2 + (\sigma_{xx}-\sigma_{yy})^2 + 4\tau_{xy}^2\right] \tag{1}$$

where G is the shear modulus and ν Poisson's ratio of the elastic and isotropic material of the strained plate.

For the case of plane-strain, expression (1) becomes:

$$\frac{dW}{dV} = \frac{1}{8G}[(1-2\nu)(\sigma_{xx}+\sigma_{yy})^2 + (\sigma_{xx}-\sigma_{yy})^2 + 4\tau_{xy}^2] \tag{2}$$

Introducing the well known relations of elasticity:

$$(\sigma_{xx}+\sigma_{yy}) = (\sigma_1+\sigma_2) \text{ and } (\sigma_{xx}-\sigma_{yy})^2 + 4\tau_{xy}^2 = (\sigma_1-\sigma_2)^2$$

relations (1) and (2) become:

$$\frac{dW}{dV} = \frac{1}{8G}[\kappa_{1,2}(\sigma_1+\sigma_2)^2 + (\sigma_1-\sigma_2)^2] \tag{3}$$

where σ_1 and σ_2 are the principal stresses corresponding to the stress tensor σ_{ij} and $\kappa_{1,2}$ take the values:

$$\kappa_1 = \frac{(1-\nu)}{(1+\nu)} \quad \text{for plane stress}$$

$$\kappa_2 = (1-2\nu) \quad \text{for plane strain} \tag{4}$$

For a thin elastic and isotropic plate, containing an inclined crack to the axes of symmetry of the plate, and submitted to a biaxial tension at infinity (Fig. 1), the complex-stress functions of Muskhelishvili [14] are given by:

$$\Phi(z) = \frac{1}{2}(2\Gamma + \bar{\Gamma}')\frac{z}{(z^2-a^2)^{1/2}} - \frac{1}{2}\bar{\Gamma}' \tag{5}$$

and

$$\Omega(z) = \frac{1}{2}(2\Gamma + \bar{\Gamma}')\frac{z}{(z^2-a^2)^{1/2}} + \frac{1}{2}\bar{\Gamma}' \tag{6}$$

where:

$$\frac{1}{2}\bar{\Gamma}' = -\frac{\sigma}{4}(1-k)\,e^{2i((\pi/2)-\omega)} \tag{7}$$

$$\frac{1}{2}(2\Gamma + \bar{\Gamma}') = \frac{\sigma}{4}[\{1 - e^{2i((\pi/2)-\omega)}\} + k\{1 + e^{2i((\pi/2)-\omega)}\}] \tag{8}$$

and a is the crack length, k is the ratio of stresses at infinity. For $k = 0$ there is uniaxial tension at infinity with the stress σ applied along the transverse boundaries of the plate, for $k = 1$ there is a biaxial tension with equal stresses σ along both pairs of boundaries of the plate, whereas for $k = -1$ there is a tension-compression state of loading at infinity with both pairs of stresses absolutely equal to σ and with opposite signs.

From relations (5) and (6) the principal stresses at the vicinity of the crack tip may

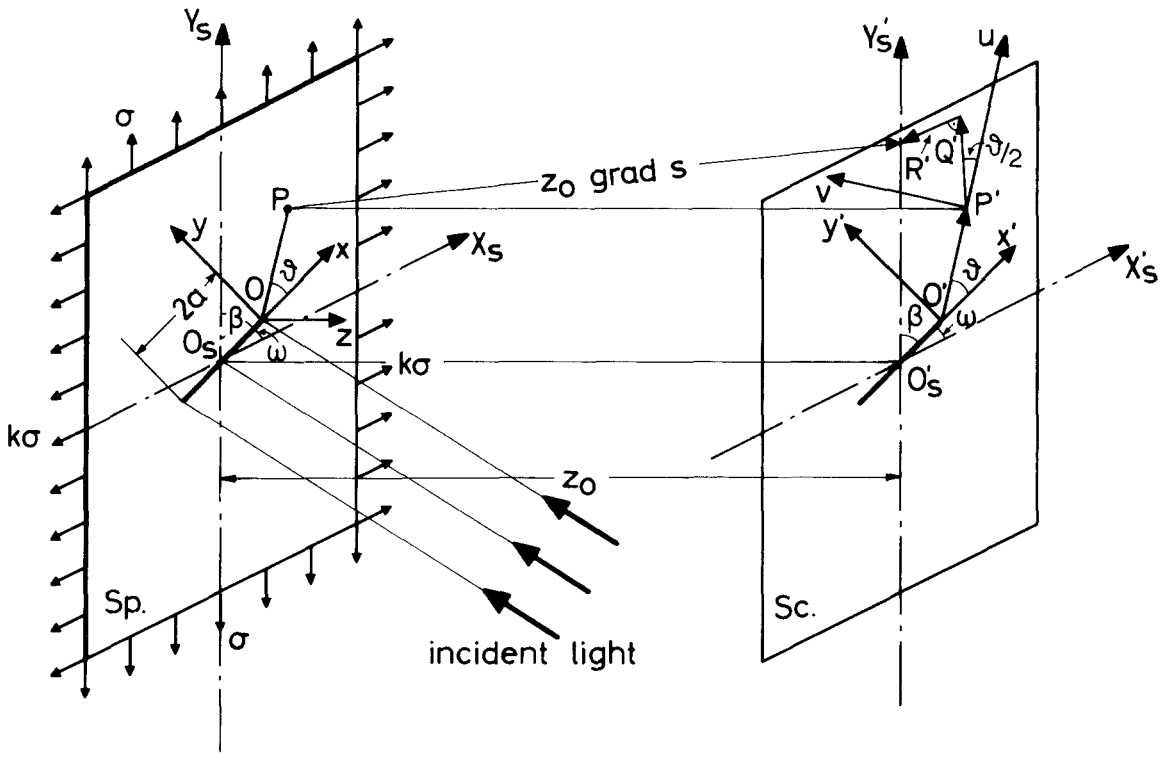

Figure 1. Geometry of cracked plate and relative position of specimen and viewing screen.

be expressed by [15]:

$$(\sigma_1+\sigma_2)=\frac{2}{(2\pi r)^{1/2}}\left(K_{\mathrm{I}}\cos\frac{\vartheta}{2}-K_{\mathrm{II}}\sin\frac{\vartheta}{2}\right)-\lambda \tag{9}$$

$$(\sigma_1-\sigma_2)=\pm\left\{\frac{1}{2\pi r}[K_{\mathrm{I}}^2\sin^2\vartheta+2K_{\mathrm{I}}K_{\mathrm{II}}\sin 2\vartheta+K_{\mathrm{II}}^2(4-3\sin^2\vartheta)]+\lambda^2+\right.$$

$$\left.+\frac{\lambda}{(2\pi r)^{1/2}}\sin\vartheta\left[K_{\mathrm{I}}\sin\frac{3\vartheta}{2}+4K_{\mathrm{II}}+2K_{\mathrm{II}}\cos\frac{3\vartheta}{2}\right]\right\}^{1/2} \tag{10}$$

where:

$$K_{\mathrm{I}}=\frac{\sigma\sqrt{\pi\alpha}}{2}[(1+k)+(1-k)\cos 2\omega] \tag{11}$$

$$K_{\mathrm{II}}=\frac{\sigma\sqrt{\pi\alpha}}{2}(1-k)\sin 2\omega \tag{12}$$

$$\lambda=\sigma(1-k)\cos 2\omega \tag{13}$$

3. The optical method of reflected caustics

Consider a monochromatic and coherent light beam, emitted from a He-Ne laser, impinging on the thin elastic transparent plate containing an oblique internal crack and submitted to a biaxial state of loading at infinity, as indicated in Fig. 1. The reflected rays from the front and rear faces of the plate are received on a ground-glass

reference-screen, placed parallel to the specimen at a distance z_0 from it. On this reference screen the reflected rays from the close vicinity of either crack tip form a caustic, whose shape is shown in Fig. 2 for uniaxial tension. The parametric equations of this strongly illuminated curve are given by [7, 16]:

$$X'_{r,f} = \left(\frac{3}{2}C_{r,f}\right)^{2/5}(K_I^2 + K_{II}^2)^{1/5}\left\{\cos\vartheta + \frac{2}{3}(K_I^2 + K_{II}^2)^{-1/2}\left(K_I\cos\frac{3\vartheta}{2} - K_{II}\sin\frac{3\vartheta}{2}\right)\right\} \tag{14}$$

$$Y'_{r,f} = \left(\frac{3}{2}C_{r,f}\right)^{2/5}(K_I^2 + K_{II}^2)^{1/5}\left\{\sin\vartheta + \frac{2}{3}(K_I^2 + K_{II}^2)^{-1/2}\left(K_I\sin\frac{3\vartheta}{2} + K_{II}\cos\frac{3\vartheta}{2}\right)\right\}$$

while the radius $r \equiv r_0$ of the generatrix curve on the specimen around the crack tip, which is the locus of the reflected rays forming the respective caustic on the reference plane Sc, is given by:

$$r \equiv r_0 = \left(\frac{3}{2\lambda_m}C_{r,f}\right)^{2/5}(K_I^2 + K_{II}^2)^{1/5} \tag{15}$$

with:

$$C_{r,f} = \frac{\epsilon z_0\, dc_{r,f}}{(2\pi)^{1/2}} \tag{16}$$

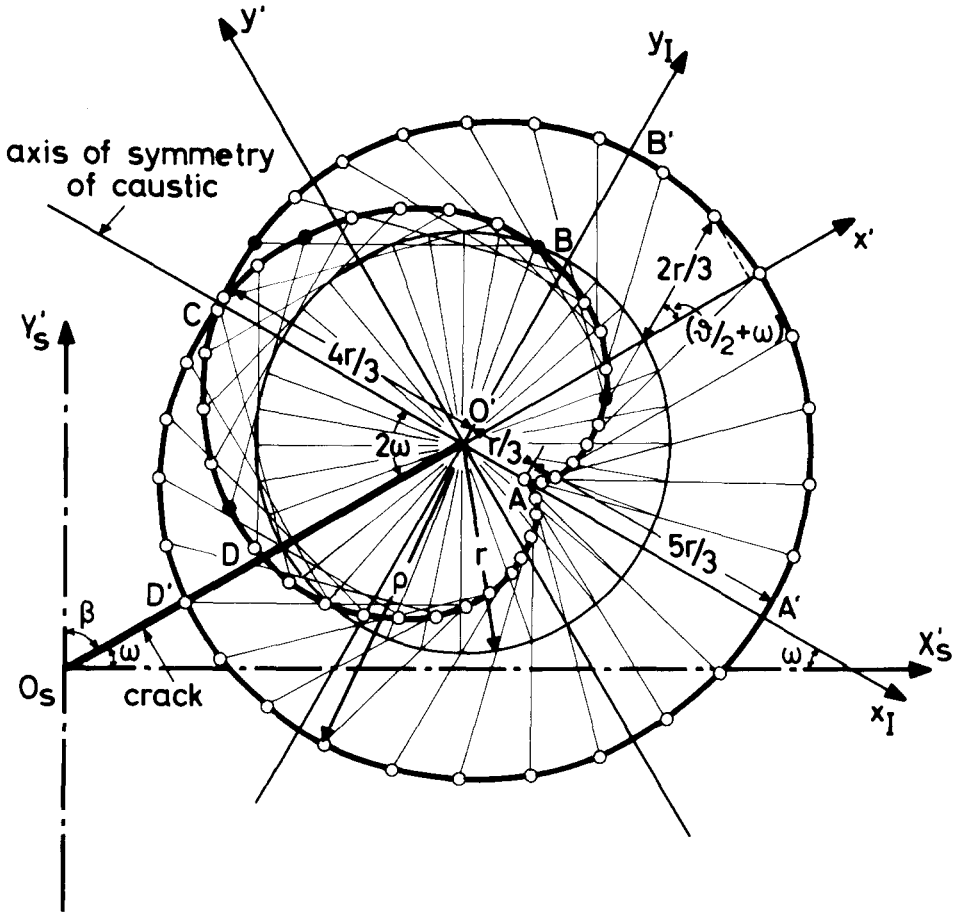

Figure 2. Shape of the principal epicycloid and geometry of its formation.

In relation (16) the quantity ϵ takes the value $\epsilon = 2$ for the reflected rays from the rear face, whereas $\epsilon = 1$ for reflections from the front face of the specimen. The subscripts r and f indicate reflections from either the rear, or the front faces, while d is the thickness of the plate and $c_{r,f}$ are the optical constants of the material of the plate again for reflections from the rear and front faces of the specimen respectively. It is worth noting here that the constant c_f for front-face reflections is independent of the optical properties of the material and equals:

$$c_f = \frac{\nu}{E}$$

where ν is the Poisson ratio and E is the elastic modulus of the material.

Moreover, the magnification ratio λ_m of the optical set-up is given by:

$$\lambda_m = \frac{z_0 \pm z_i}{z_i} \tag{17}$$

where z_i is the distance between the focus of the light beam and the middle plane of the specimen, while the positive sign is taken for a real image of the plate on the screen and the negative sign for a virtual image.

The coincidence of the boundary of the singular core with the initial curve may be explained as follows: during the loading of the cracked plate a dimple is created surrounding the crack-tip, which has the form presented in Fig. 3, if tension is predominant. This dimple presents a particular zone, where the slope of the thickness-variation of the specimen presents inflection points. Outside this limit curve strict linear elasticity is dominating, while, inside this curve, non-linear elasticity (or even plasticity in ductile materials) is progressively intervening to reduce the continuous increase of the gradient of the lateral deformation of the specimen as one approaches the singularity.

This inflection zone, surrounding the crack tip, makes the impinging light rays to

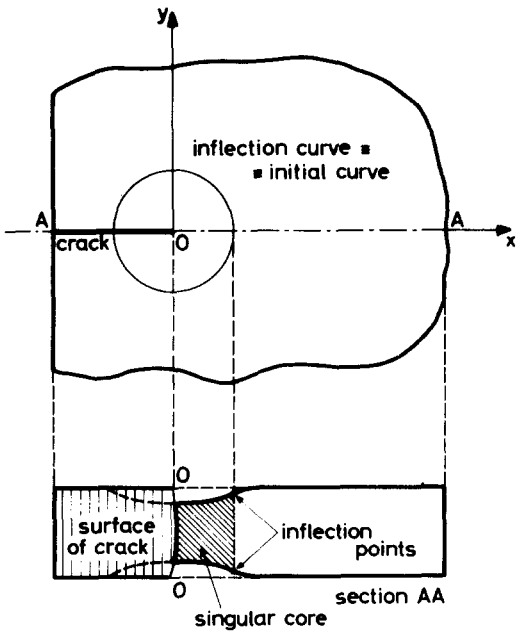

Figure 3. The shape of the inflection area surround of the crack's tip.

bend back, when reflected on the faces of the specimen, and this creates the caustic. Thus, this zone coincides with the initial curve, as defined previously. Therefore, it is reasonable to assume that the singular core extends out to this limiting curve, since this is the boundary inside of which non-linear elasticity is dominant.

If one compares the size of the singular core as defined by previous researchers [13] which is of the order of 0.002 in.and the radii of the initial curves of our caustics which are usually of the order of 0.1 mm. their coincidence in size is striking.

Solving Eqs. (14) and (16) for K_I for $k = 0$ (uniaxial tension) we obtain:

$$K_I = \frac{2(2\pi)^{1/2}}{3\epsilon z_0 d c_{r,f} \lambda_m^{3/2}} \left(\frac{D_{T,L}^{max}}{\delta_{T,L}^{max}}\right)^{5/2} \tag{18}$$

and

$$K_{II} = K_I \tan \omega \tag{19}$$

In these relations D_T^{max} and D_L^{max} are the maximum transverse- and longitudinal-diameters of the caustic and δ_T^{max} and δ_L^{max} the correction factors for D_T^{max} and D_L^{max} respectively given by the nomogram of Fig. 4 [16] for $k = 0$ (uniaxial tension).

Relations (14) and (16) indicate that when both stress intensity factors are operative ($\mu \neq 0$), the caustic is angularly displaced by an angle -2ω relatively to the crack-axis, where angle ω is defining the angle of inclination of the crack shown in Fig. 2.

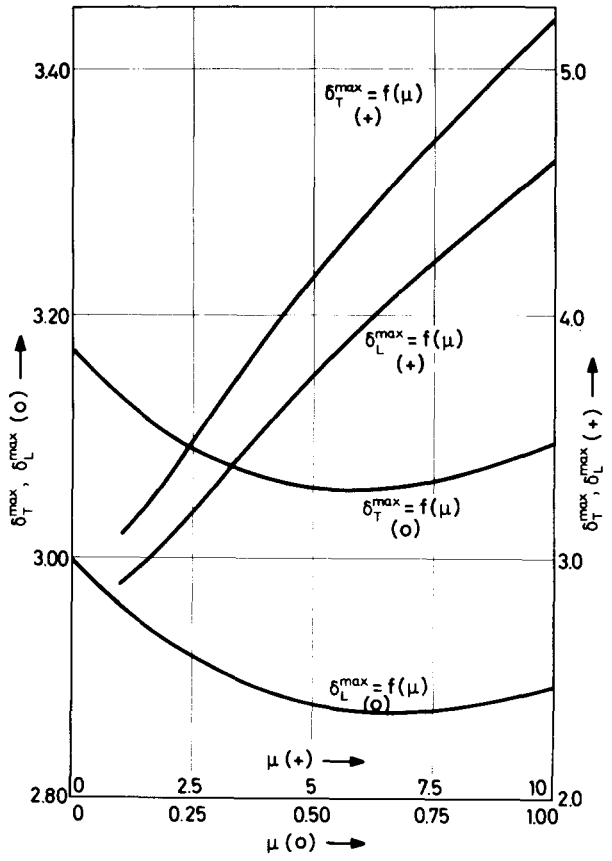

Figure 4. Variation of transverse and longitudinal correction factors δ_T^{max} and δ_L^{max} *versus* μ.

4. Evaluation of the elastic-strain-energy density from the diameters of the caustic

Using relations (15) and (16), relations (9) and (10), which give the sum and the difference of principal stresses, may be written as follows:

$$(\sigma_1 + \sigma_2) = \frac{2f}{(K_I^2 + K_{II}^2)^{1/10}} \left(K_I \cos\frac{\vartheta}{2} - K_{II} \sin\frac{\vartheta}{2} \right) - \lambda \tag{20}$$

and

$$(\sigma_1 - \sigma_2) = \pm \left\{ \frac{f^2}{(K_I^2 + K_{II}^2)^{1/5}} [K_I^2 \sin^2\vartheta + 2K_I K_{II} \sin 2\vartheta + K_{II}^2(4 - 3\sin^2\theta)] + \lambda^2 + \right.$$
$$\left. + \frac{f\lambda}{(K_I^2 + K_{II}^2)^{1/10}} \sin\vartheta \left(K_I \sin\frac{3\vartheta}{2} + 4K_{II} + 2K_{II} \cos\frac{3\vartheta}{2} \right) \right\}^{1/2} \tag{21}$$

where

$$f = (2\pi)^{-1/2} \left(\frac{3}{2} \frac{C_{r,f}}{\lambda_m} \right)^{-1/5} \tag{22}$$

Introducing relations (20) and (21) into Eq. (3) we obtain:

$$8G \frac{dW}{dV} = \frac{f^2}{(K_I^2 + K_{II}^2)^{1/5}} \left[4\kappa_{1,2} \left(K_I \cos\frac{\vartheta}{2} - K_{II} \sin\frac{\vartheta}{2} \right)^2 + K_I^2 \sin^2\vartheta + 2K_I K_{II} \sin 2\vartheta \right.$$
$$\left. + K_{II}^2(4 - 3\sin^2\vartheta) \right] - \frac{\lambda f}{(K_I^2 + K_{II}^2)^{1/10}} \left[4\kappa_{1,2} \left(K_I \cos\frac{\vartheta}{2} - K_{II} \sin\frac{\vartheta}{2} \right) \right.$$
$$\left. - \sin\vartheta \left(K_I \sin\frac{3\vartheta}{2} + 4K_{II} + 2K_{II} \cos\frac{3\vartheta}{2} \right) \right] + \lambda^2(1 + \kappa_{1,2}) \tag{23}$$

Relation (23) gives the distribution of the elastic strain energy density along a small circle representing the singular core, coinciding with the initial curve of the caustic and surrounding the crack tip, when the cracked plate is submitted to a biaxial state of loading at infinity and both K_I and K_{II} are operative. For isotropic, elastic and optically-inert materials the initial circle has a radius r_0 given by relation (15).

It has been shown in ref. [8], and from the previously developed theory, that the size of this circle may be chosen as small as desirable, by decreasing the overall optical constants $C_{r,f}$ and increasing the magnification ratio λ_m. This possibility allows the evaluation of the elastic-strain-energy distribution around the crack tip along a well defined curve, that is the initial curve which lies as close as possible to the crack tip.

Relation (23) was used to trace on a digital computer and plotter the elastic-strain-energy density distribution around a crack tip in a plexiglas plate with $\nu = 0.34$, d = 0.003 m, $c_r = -3.3 \times 10^{-10}$ m^2/N, $2\alpha = 0.02$ m, $\sigma = 1$ N/m^2, $\epsilon = 2$, $z_0 = 2$ m, $z_i = 0.5$ m and $\lambda_m = 5$. Figs. 5(a and b) present various distributions of the elastic strain energy density for plane-stress conditions of the cracked plate when the loading ratio k varies between -1 and 1 for $\omega = 0°$, 30°, 45°, (Fig 5a) and $\omega = 60°$, 70° and 80° (Fig. 5b).

The influence of the loading-ratio k, as well as the angle ω on the distribution of the elastic-strain-energy density is clear from these figures. It is worthwhile indicating that the ESED-distribution presents always a minimum in front of the crack tip, whose position and magnitude vary in terms of k and ω. It is clear from Figs. 5(a and b) that, while the magnitude of this minimum depends mainly on k, its position depends exclusively on ω.

The position of this minimum (ϑ_{min}) may be defined by annulling the partial

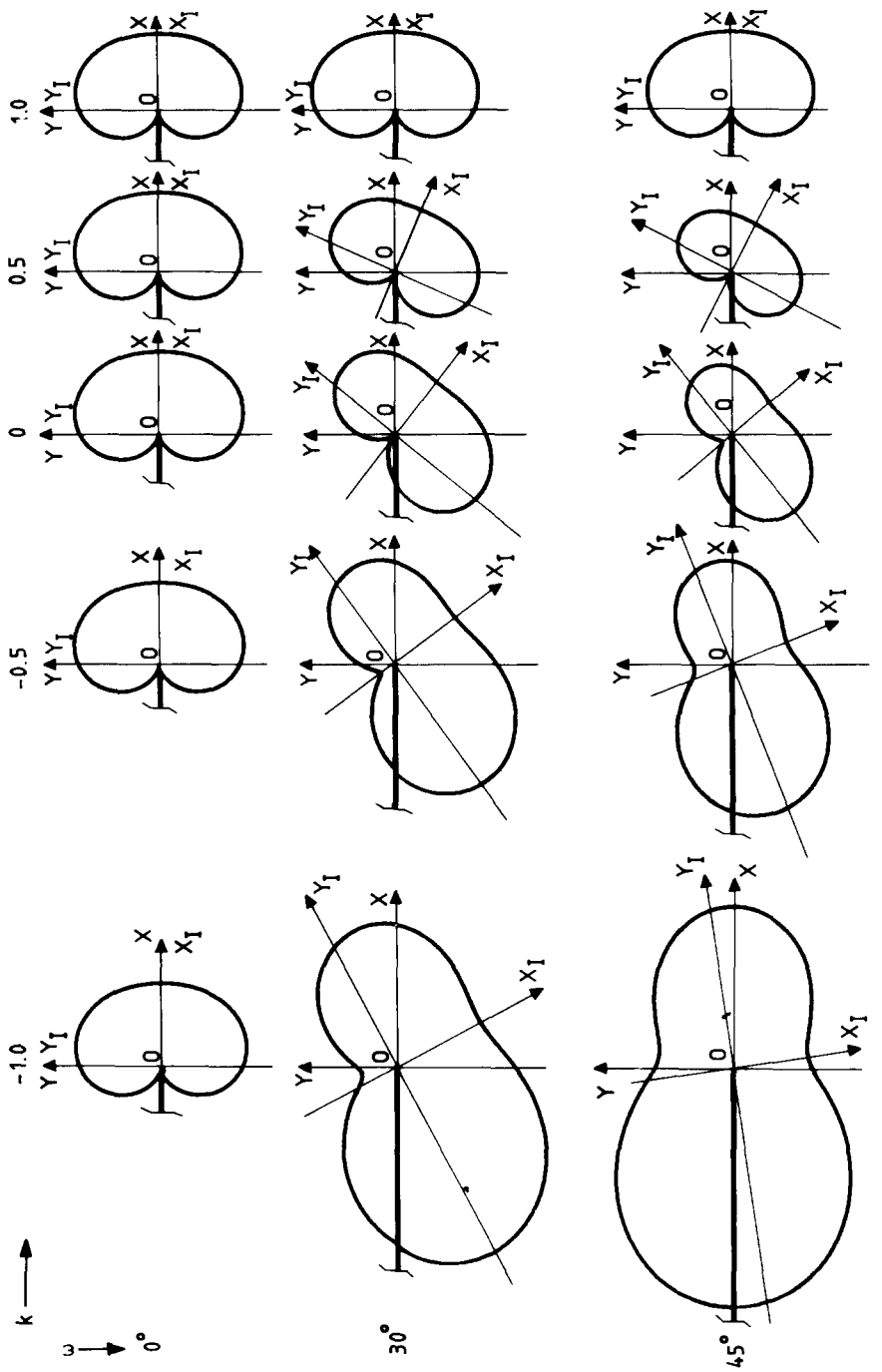

Figure 5a. Plotting of the distribution of the elastic strain-energy density at the crack tip for k between -1 and 1 and for $\omega = 0°, 30°$ and 45° and for plane-stress conditions.

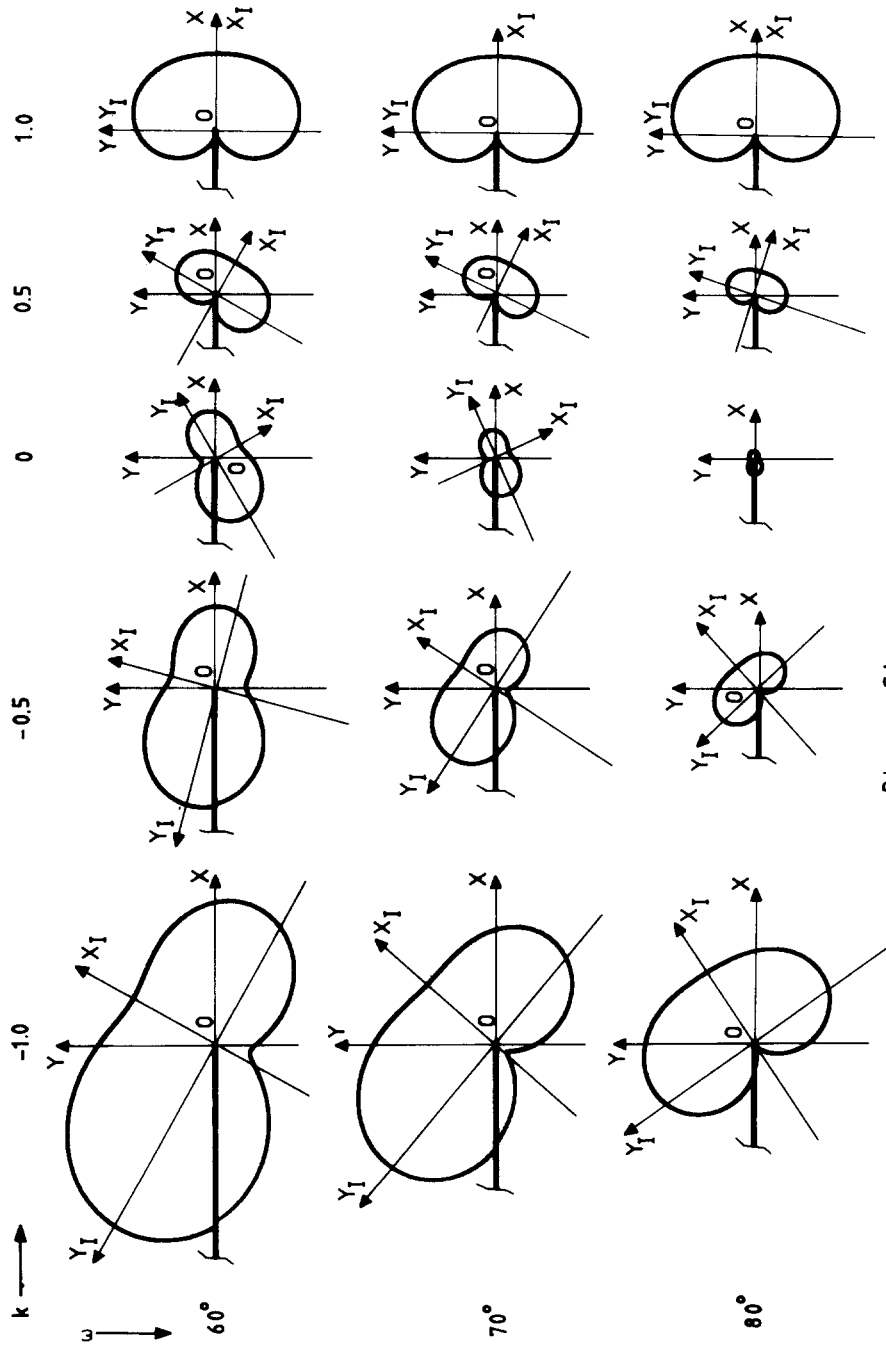

Figure 5b. Plotting of the distribution of the elastic strain-energy density at the crack tip for k between -1 and 1 for $\omega = 60°$, 70° and 80° and for plane-stress conditions.

derivative $\partial/\partial\vartheta$ (dW/dV). By differentiating relation (23), one obtains the relation:

$$8G\frac{\partial}{\partial\vartheta}\left(\frac{dW}{dV}\right)=\frac{f^2}{(K_I^2+K_{II}^2)^{1/5}}\{-2\kappa_{1,2}[(K_I^2-K_{II}^2)\sin\vartheta+2K_IK_{II}\cos\vartheta]$$
$$+(K_I^2-3K_{II}^2)\sin 2\vartheta+4K_IK_{II}\cos 2\vartheta\}+$$
$$+\frac{\lambda f}{(K_I^2+K_{II}^2)^{1/10}}\left\{2\kappa_{1,2}\left(K_I\sin\frac{\vartheta}{2}+K_{II}\cos\frac{\vartheta}{2}\right)\right.$$
$$+\cos\vartheta\left(K_I\sin\frac{3\vartheta}{2}+2K_{II}\cos\frac{3\vartheta}{2}+4K_{II}\right)$$
$$\left.+\frac{3}{2}\sin\vartheta\left(K_I\cos\frac{3\vartheta}{2}-2K_{II}\sin\frac{3\vartheta}{2}\right)\right\}=0 \qquad (24)$$

Figures 6(a and b) present the variation of ϑ_{min} *versus* ω for parametric values of the loading ratio k for plane stress (Fig. 6a) or plane strain (Fig. 6b). In both cases the values of ω vary between 0° and 90°.

Figures 7(a and b) present the variations of ϑ_{min} versus the loading ratio k with ω as a parameter for plane-stress (Fig. 7a) or plane-strain (Fig. 7b).

Introducing the value for ϑ_{min} into relation (23), one obtains the values of the

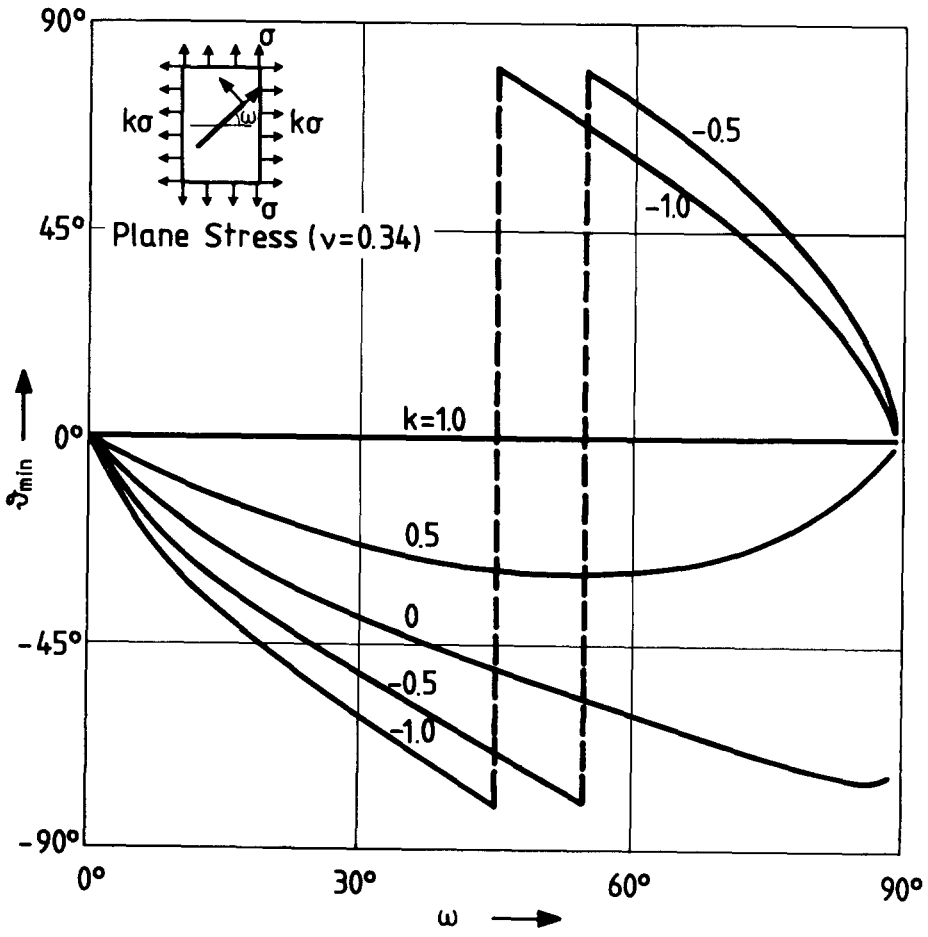

Figure 6a. Variation of ϑ_{min} *versus* ω for various parametric values of k for plane-stress conditions.

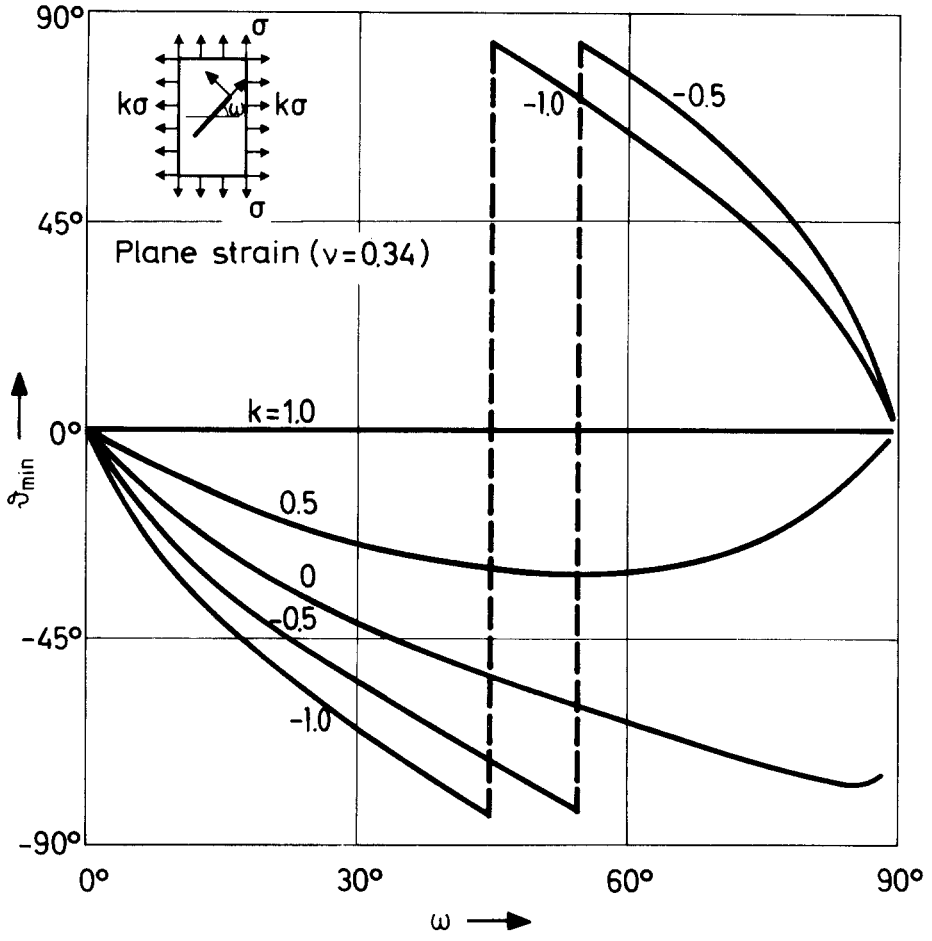

Figure 6b. Variation of ϑ_{min} *versus* ω for various parametric values of k for plane-strain conditions.

minimum of the elastic-strain-energy density $(dW/dV)_{min}$ given by:

$$8G\left(\frac{dW}{dV}\right)_{min} = \frac{f^2}{(K_I^2+K_{II}^2)^{1/5}}\left[4\kappa_{1,2}\left(K_I\cos\frac{\vartheta_{min}}{2}-K_{II}\sin\frac{\vartheta_{min}}{2}\right)^2+K_I^2\sin^2\vartheta_{min}\right.$$
$$\left.+2K_IK_{II}\sin 2\vartheta_{min}+K_{II}^2(4-3\sin^2\vartheta_{min})\right]$$
$$-\frac{\lambda f}{(K_I^2+K_{II}^2)^{1/10}}\left[4\kappa_{1,2}\left(K_I\cos\frac{\vartheta_{min}}{2}-K_{II}\sin\frac{\vartheta_{min}}{2}\right)\right.$$
$$\left.-\sin\vartheta_{min}\left(K_I\sin\frac{3\vartheta_{min}}{2}+2K_{II}\cos\frac{3\vartheta_{min}}{2}+4K_{II}\right)\right]+\lambda^2(1+\kappa_{1,2}) \qquad (25)$$

Figures 8(a and b) present the variation of the minimum of the elastic-strain-energy density $(dW/dV)_{min}$, normalized to the respective minimum for $\omega = 0$ and $k = 0$ (transverse crack for uniaxial tension, $K_{II} = 0$), *versus* ω for various parametric values of k and for plane-stress (Fig. 8a), or plane-strain (Fig. 8b) conditions of the cracked plate. Figs. 9(a and b) present the variation of the same minimum $(dW/dV)_{min}$ normalized to the same respective minimum for $\omega = 0$ and $k = 0$ *versus* the loading ratio k for various parametric values of ω and again for plane stress (Fig. 9a), or plane-strain (Fig. 9b) conditions.

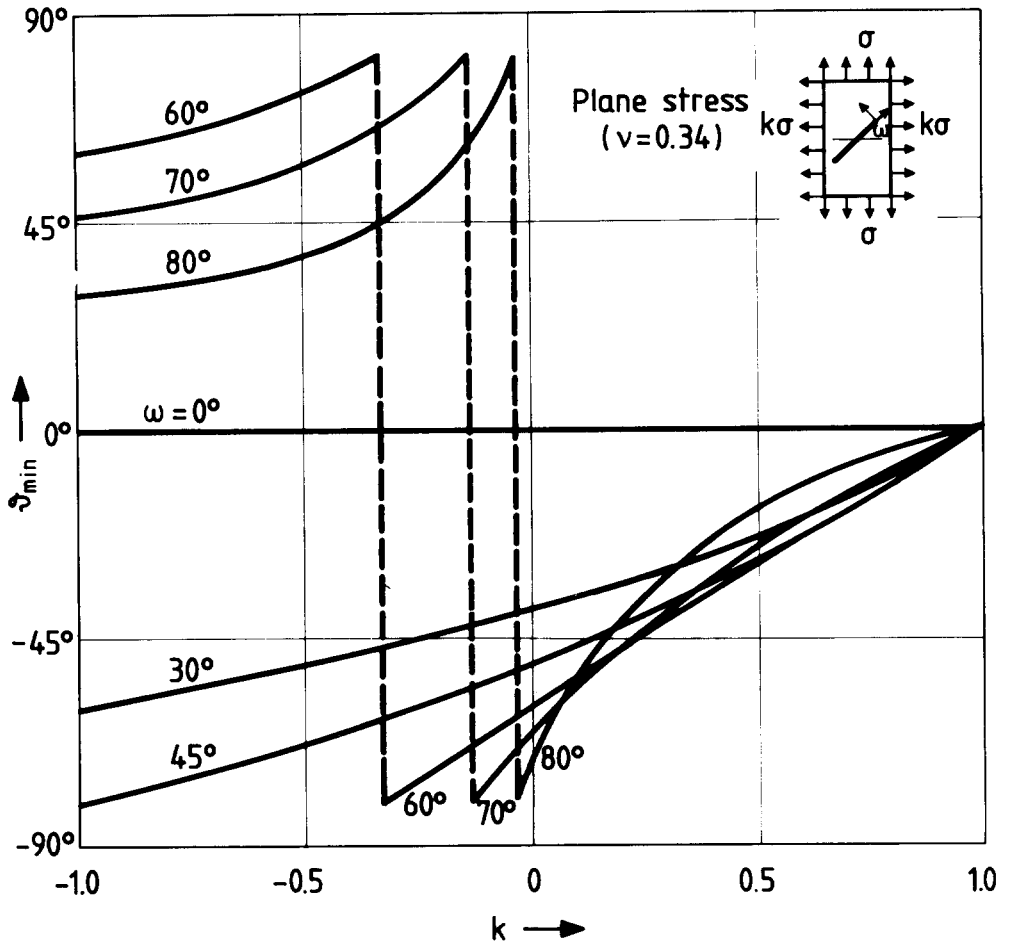

Figure 7a. Variation of ϑ_{min} *versus* k for various parametric values of ω and for plane-stress conditions.

The distribution of the strain energy density is symmetric relatively to the crack axis for $\omega = 0$ for every value of k, and for $k = 1$ for every value of ω, as it has been already indicated in Figs 5(a, b). This symmetric distribution ceases to exist as soon as ω and k takes values different than zero and 1 respectively. In these cases the lobe of the distribution of the energy density is angularly displaced by an angle $-\vartheta_{min}$ and, besides this rotation, there is also an asymmetric distribution of the energy density in the two semi-lobes. Indeed, it can be readily derived from Figs. 5(a, b) that the size of the lobe representing the distribution of the elastic energy density depends on both quantities ω and k.

If E_1 and E_2 represent the areas of the upper and lower parts of the energy-density lobe, as it has been divided by the straight line connecting the crack tip with the point of minimum density, these areas may be calculated by evaluating the following integrals:

$$E_1 = \frac{1}{2}\int_{\vartheta_{min}}^{(\pi+\vartheta_{min})} \left(\frac{dW}{dV}\right)^2 d\vartheta \quad \text{and} \quad E_2 = \frac{1}{2}\int_{-\pi+\vartheta_{min}}^{\vartheta_{min}} \left(\frac{dW}{dV}\right)^2 d\vartheta \tag{26}$$

The variation of the ratio E_1/E_2 in terms of ω is given in Figs. 10a for plane-stress and 10b for plane-strain conditions of the cracked plate, for k as a parameter, while

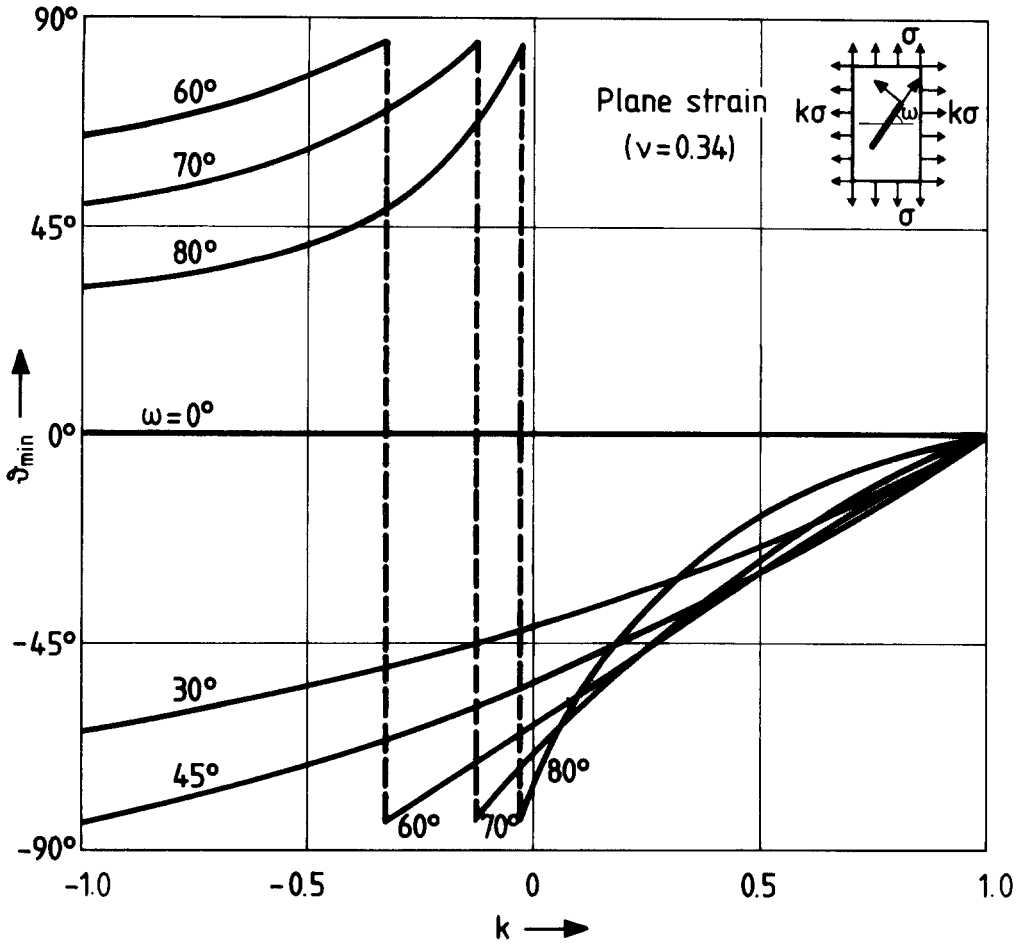

Figure 7b. Variation of ϑ_{min} *versus* k for various parametric values of ω and for plane-strain conditions.

the variation of the ratio E_1/E_2 is plotted *versus* k in Fig. 11a for plane-stress and Fig. 11b for plane-strain conditions for ω as a parameter. Furthermore, the variation of the total area $E = (E_1 + E_2)$ of the lobe of distribution of energy density normalized to the area $E^{\omega,k=0}$ of the respective lobe for $\omega = 0$ and $k = 0$ *versus* either the angle ω, or the loading ratio k is given in Figs. 12(a and b) and 13(a and b) respectively, again, for plane-stress and plane-strain conditions.

5. Results

The experimental study of Sih's criterion for the propagation of a crack and the direction of the minimum elastic-strain energy density in a plate under plane-stress conditions and submitted to a general biaxial-type of loading at infinity indicated that the strain-energy density distribution depends on the angle of inclination of the crack ω, as well as on the loading ratio k (Figs. 5(a and b)). The position of the minimum elastic-strain energy density, defined by angle ϑ_{min}, and therefore the direction of propagation of the crack depends on ω and k (as it may be concluded from Figs. 6(a, b) and Figs. 7(a, b)). For $k \geqq 0$ and for ω varying between 0° and 90°, $|\vartheta_{min}|$ increases and, after having passed from a maximum, it decreases and tends to 0°, for $k = 1$, $\vartheta_{min} = 0$. This means that for whatever angle ω the crack will spread straight

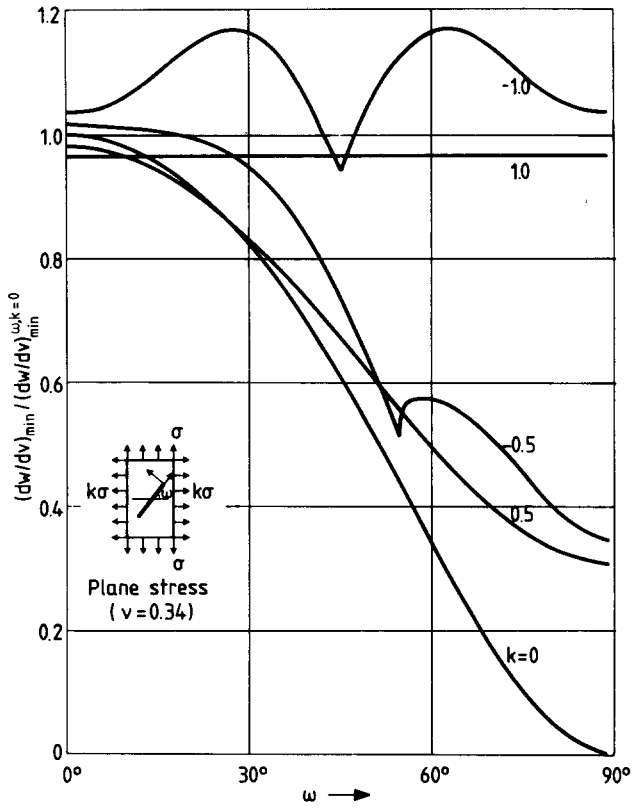

Figure 8a. Variation of the minimum of the ESED $(dW/dV)_{min}$, normalized to the respective minimum for $\omega = 0$ and $k = 0$ (transverse crack for uniaxial tension, $K_{II} = 0$) *versus* ω, for various parametric values of k and for plane-stress conditions.

ahead because $K_{II} = 0$. For $k < 0$ the angle $|\vartheta_{min}|$ increases and for values of $\omega \geqq 45°$ there exist values of k yielding $K_I = 0$ and $K_{II} \neq 0$ (pure shear). At these positions of pure shear a change of sign of ϑ_{min} appears and then a decrease of its value tending to 0° for ω tending to 90° is detected. The change of values of minimum strain-energy density, normalized to the value of minimum strain-energy density for $\omega = 0$ and $k = 0$ (uniaxial tension, $K_{II} = 0$), is shown in figures 8a, 8b, as well as in Figs 9a and 9b. For $k = 0$ the values of minimum strain-energy density decrease rapidly tending to 0° as ω tends to 90°. For $k > 0$ they continuously decrease without tending to zero because K_{II} remains always different than zero for all angles ω. For $k = 1$ ($K_{II} = 0$) the value of the minimum strain-energy density remains constant. For $k < 0$ the values decrease up to $\omega = 45°$ and after passing from a minimum, which corresponds to the positions of pure shear ($K_I = 0$), they increase and afterwards decrease again. For $k = -1$ a symmetrical distribution of the energy density appears with an axis of symmetry at 45°.

A measure of the influence of ω and k to the position of ϑ_{min} for the minimum of the strain-energy density for plane-stress and plane-strain is given by the distribution of the area of the lobe defined by the curve of the distribution of the strain-energy density around the crack tip.

Figures 10(a, b) and 11(a, b) present the variation of the ratio E_1/E_2 of the areas of the upper and lower semi-lobes divided by the axis of ϑ_{min}. From Figs. 10(a, b) and 11(a, b) it can be seen that for $k = 1$ and for all angles ω the lobe-area distribution is symmetric to the direction of minimum strain-energy density. For $k \geqq 0$ the ratio E_1/E_2 decreases and after passing from a minimum, lying in between 30° and 60°,

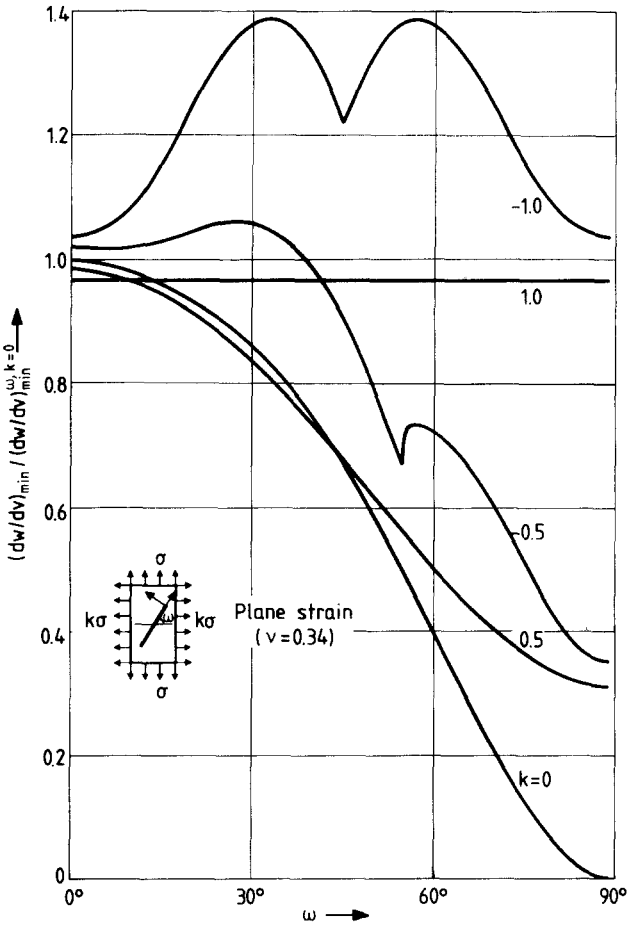

Figure 8b. Variation of the minimum of the E.S.E.D $(dW/dV)_{min}$, normalized to the respective minimum for $\omega = 0$ and $k = 0$ (transverse crack for uniaxial tension, $K_{II} = 0$) *versus* ω, for various parametric values of k and for plane-strain conditions.

increases again and tends to unity for ω tending to 90°. For $k < 0$ the ratio E_1/E_2 decreases again up to $\omega = 45°$. For angles $\omega \geqq 45°$, corresponding to positions of pure shear ($K_I = 0$) and changes of sign of ϑ_{min}, a reversion of the magnitudes of areas E_1 and E_2 is observed and consequently the ratio E_1/E_2 becomes greater than unity and after passing from a maximum tends to unity as ω tends to 90°.

Figures 12(a, b) and 13(a, b) yield the influence of ω and k on the total area of the surface E included in the lobe of the energy density distribution, normalized to the area corresponding to uniaxial tension ($k = 0$) for $\omega = 0$, for plane stress and plane strain conditions. This influence is small for small values of $\omega(\omega < 10°)$. Above this region it becomes more and more important. The area E increases for $k < 0$, while for $k > 0$ it diminishes, and after passing a minimum it, again, increases.

6. A model for the propagation mode of cracks for $k = 0$ (uniaxial tension).

In this section a model for the propagation mode of a crack is proposed, based on the minimum strain-energy criterion. The validity of this model is checked with the method of reflected caustics.

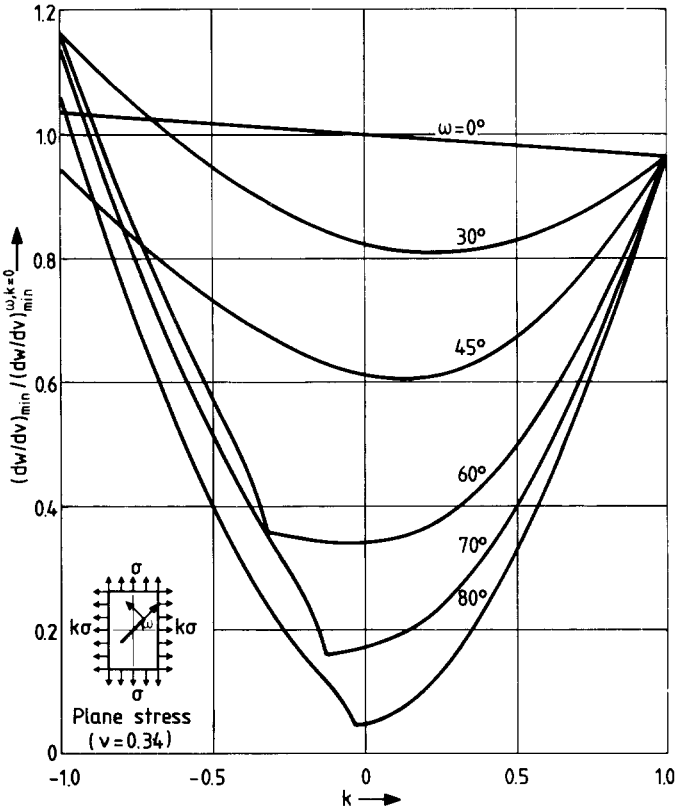

Figure 9a. Variation of the minimum of the ESED $(dW/dV)_{min}$, normalized to the respective minimum for $\omega = 0$ and $k = 0$ (transverse crack for uniaxial tension, $K_{II} = 0$) *versus* k, for various parametric values of ω and for plane-stress conditions.

The zig-zag path of a propagating crack in a plate under tension may be explained by considering the advancement of a crack as consisting of distinctive steps, where voids and other discontinuities of the material, surrounding the crack-tip, coalesce and create each kink for the crack. In such a case it is assumed that the crack propagates along the direction of minimum strain-energy density.

Figure 14 shows the initial crack with its tip at O_1 and successive kinks O_1O_1, O_1O_2, O_2O_3, ... Although the singularity existing at the tip of the crack for each position dominates the stress field at the vicinity of the tip, there are also weaker singularities existing at the successive corners O_1, O_1, O_2, O_3, ..., each of which is influencing the state of stress at the crack tip when this crack is still at the neighbourhood of this corner [18, 19].

It is known that the singularity at a multiwedge, as is the case at each corner with the branches of the crack separating the material in several wedges, diminishes as the convex angle at the corner is diminishing and becomes equal to zero when this angle tends to 180°. When the crack propagates along the kink after the corner O_1 the new crack forms an angle with the axis of the previous step lying between 220° and 255°, depending on the value of angle ω (Fig. 15). For such angles the order of singularity lies between -0.3 and -0.4 and, therefore, it is quite large, as compared with the singularity at the tip of the new crack, which is of the order -0.5. The singularity of the corner interacts with the singularity at the crack tip and this results in a progressive bending of the crack at the vicinity of each corner. Then, the real crack path is as shown in Fig. 16 with the dotted lines indicating the transition periods at

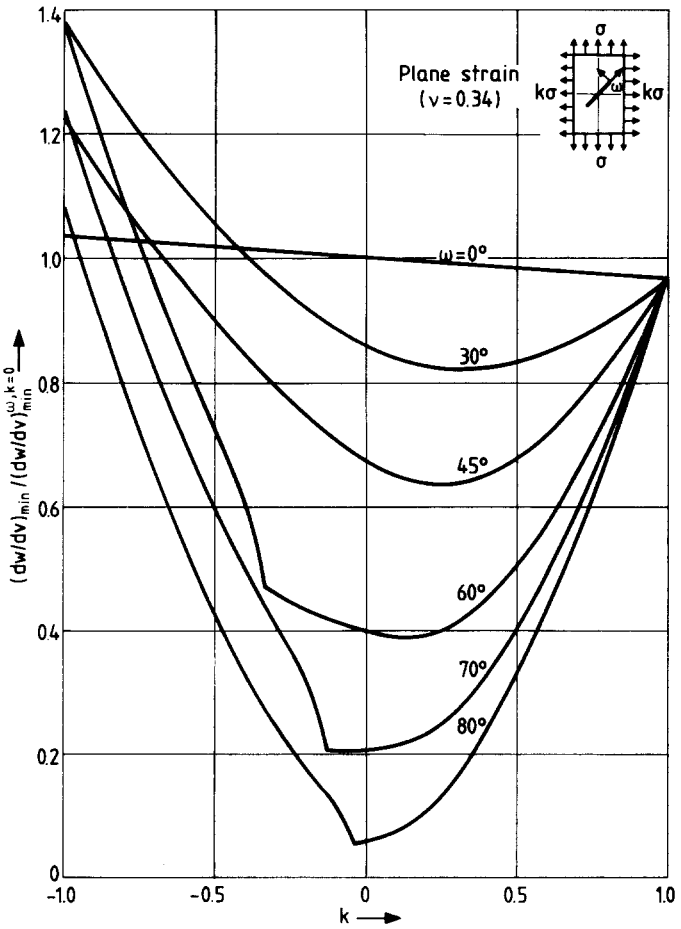

Figure 9b. Variation of the minimum of the ESED $(dW/dV)_{min}$, normalized to the respective minimum for $\omega = 0$ and $k = 0$ (transverse crack for uniaxial tension, $K_{II} = 0$) *versus* k, for various parametric values of ω and for plane-strain conditions.

each corner of the zig-zag crack. This continuous bending of the crack diminishes as the crack-tip recedes from the neighboring corner, since the influence of the singularity of the corner on the singularity of the crack tip becomes weaker with distance.

Figure 17a presents a branched crack in a polycarbonate thick tension specimen, where many branches and kinks present this progressive bending after their passing from a corner. Fig. 17b presents the same crack photographed in oblique angle so that the shape of the branches through the thickness of the specimen are more apparent.

In the next step, after the corner point O_1, the angle ϑ is of the order of 190° and 200° and the singularity at the corner is of the order −0.1 and −0.2. Its influence, therefore, on the mode of propagation of the next kink is smaller than in the previous step. The next corner O_2 creates a multiwedge with an angle not overpassing 190° and therefore the influence of the singularity of this corner (−0.1) on the crack-tip singularity is further diminished and it may be neglected.

The initial bending and angular displacement of the crack axis at the various steps of crack propagation in clearly indicated in Fig. 17 where the microbranches of the main crack developed at various steps of its propagation are at the beginning bent

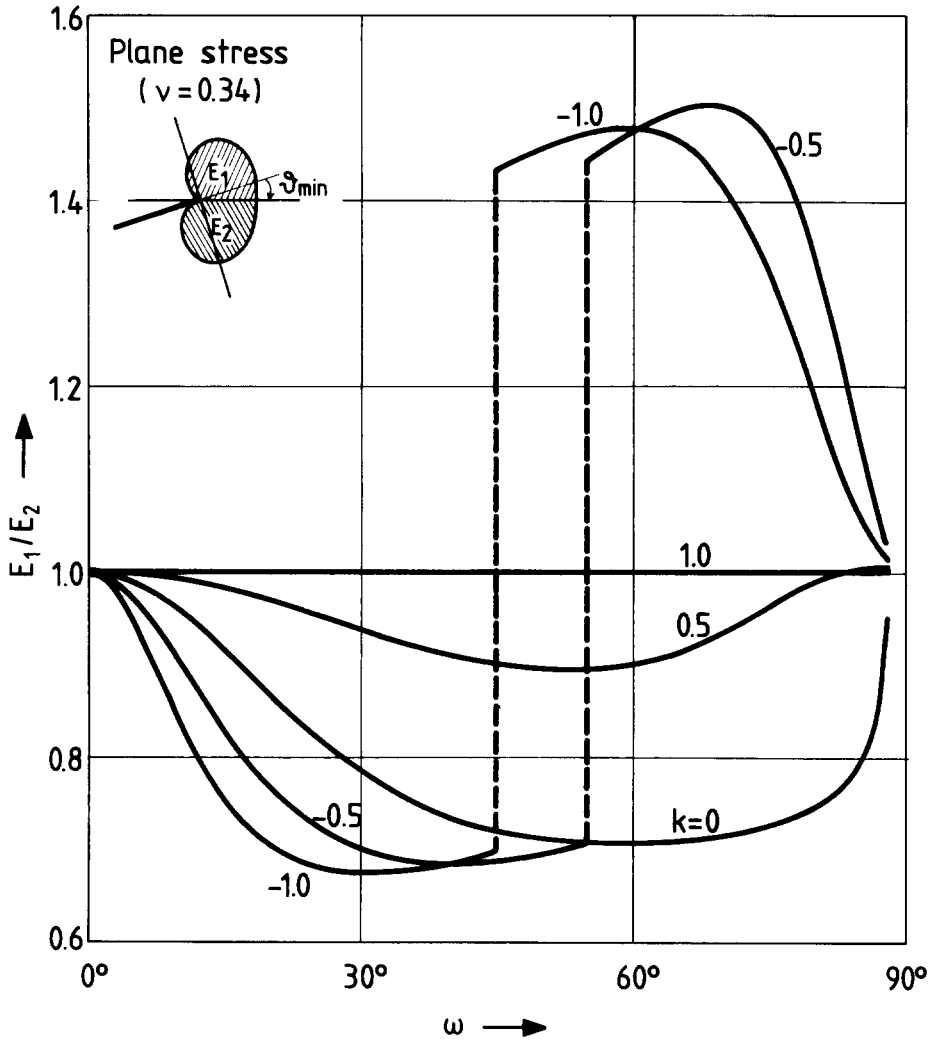

Figure 10a. Variation of the ratio E_1/E_2 *versus* ω for various parametric values of k and for plane-stress conditions.

progressively and they tend afterwards to propagate along straight lines forming different angles with the axis of the main crack.

Figure 18 presents the details of rotation of the crack axis in a plexiglas plate subjected to simple tension and containing an initial oblique crack of a length $a = 0.010$ m. at an angle $\omega = 45°$. The reflected caustics formed at each position of the crack tip have different orientations relatively to the axis of the initial crack indicating the zig-zag progress of the crack, as it recedes from the corner point O, corresponding to the tip of the initial crack. As the crack tip recedes from the corner O the direction of the crack stabilizes to a constant angle.

In the reflected caustics of this figure the external branches of each caustic correspond to reflections from the rear face of the specimen, whereas the internal branches to reflections from the front face. It is previously shown that the cusped internal caustics yield immediately the direction of the crack axis by tracing the mid-normal to the tangent of the two lobes of the cusp. In this way we may define

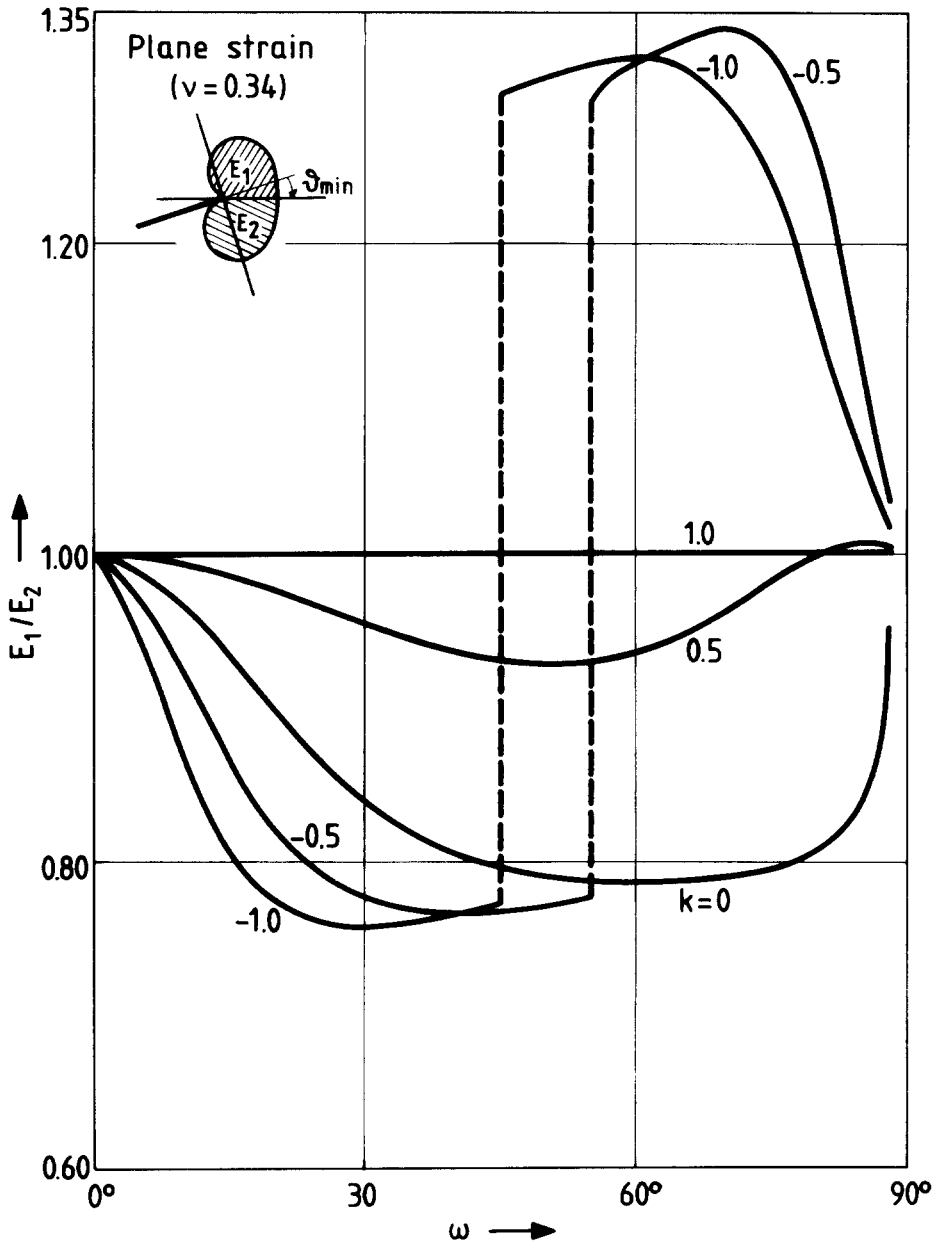

Figure 10b. Variation of the ratio E_1/E_2 *versus* ω for various parametric values of k and for plane-strain conditions.

rapidly and accurately the actual inclination of the crack axis and compare it with the corresponding angle of the model.

If an edge crack of an initial length a forms an angle ω with the transverse axis (Ox-axis) of a long strip subjected to simple tension, application of a stress σ at infinity engenders a strain energy concentration at the crack tip, whose density is given by relation (23).

The distribution of the elastic-strain energy along the boundary of the singular core, which coincides with the area limited by the initial curve of the caustic (and which is always a circle of radius r_0 for isotropic elastic materials and small scale

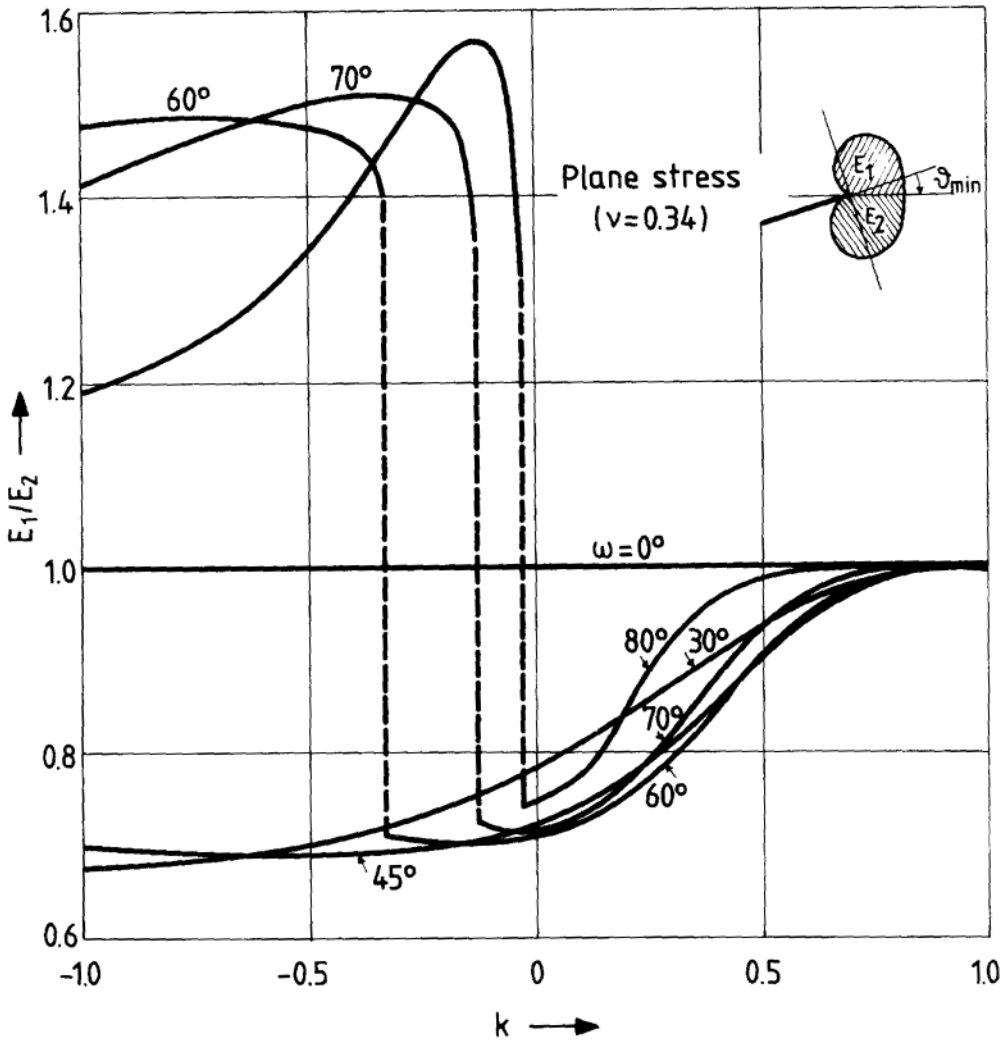

Figure 11a. Variation of the ratio E_1/E_2 *versus* k for various parametric values of ω and for plane-stress conditions.

yielding), always presents a minimum at the radius subtending an angle $(-\vartheta_{min})$ with the crack-axis (O_1x_1-axis of Fig. 14). The position of this minimum direction is defined by relation (24). According to the criterion of the minimum elastic strain energy density the crack will propagate along a direction O_1O_1 which is subtending an angle $-\vartheta_{min,1}$ with the old crack axis (O_1X_1) and the crack in its new axis propagates along the length O_1O_1. Now, in its new position the crack subtends an angle $-|\vartheta_{min,1}-\omega|$ with the transverse Ox-axis of the strip.

In this new position the SIF ratio μ is given by:

$$\mu = \frac{K_{II}}{K_I} = -\tan|\vartheta_{min,1}-\omega| \tag{27}$$

and this ratio implies the strain energy density lobe to be angularly displaced by an angle $+\vartheta_{min,2}$ relatively to the crack-axis (O_1O_1-axis). Therefore according to the density criterion the new crack path is along O_1O_2 subtending an angle $\vartheta_{min,2}$ with the

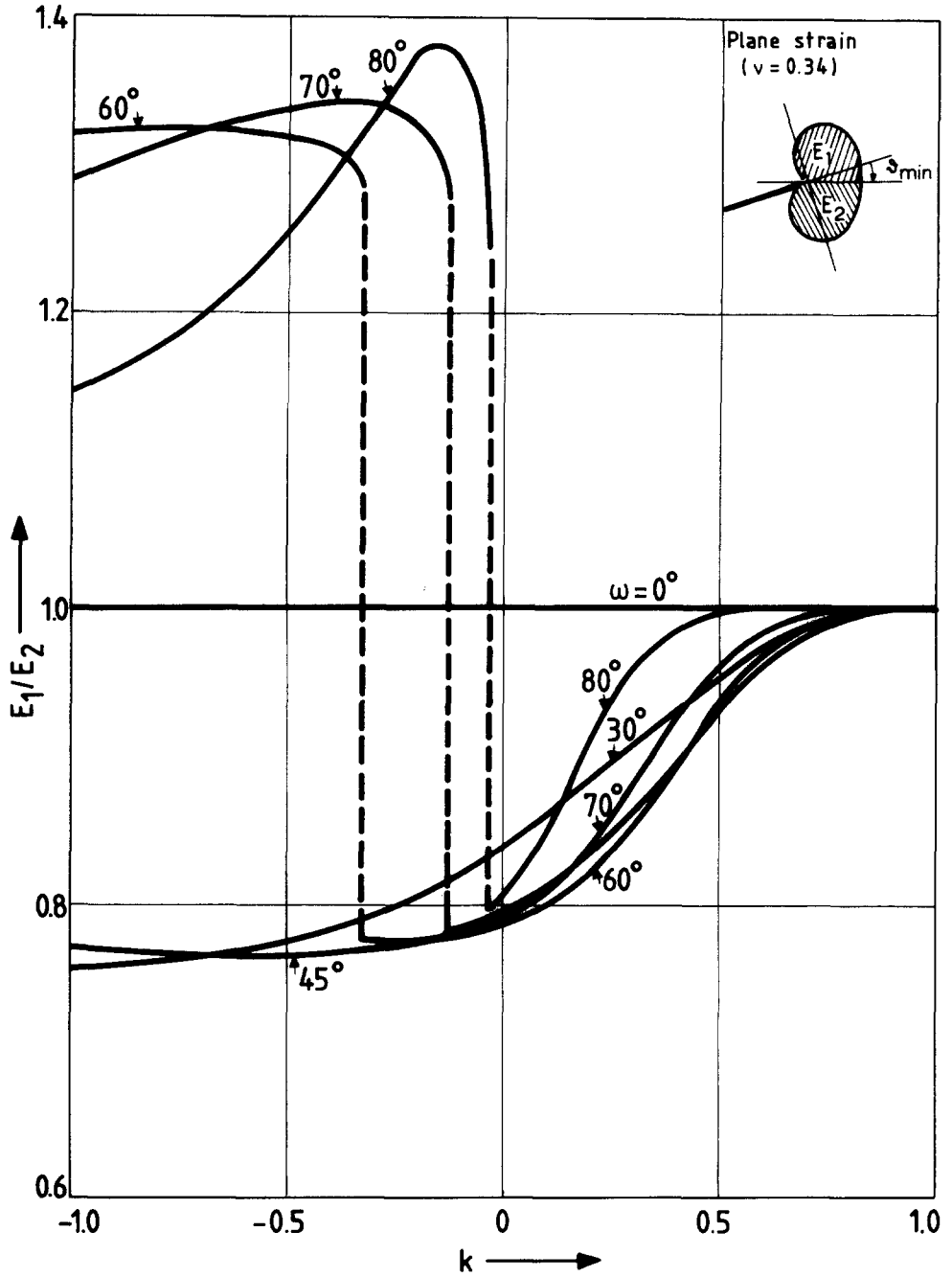

Figure 11b. Variation of the ratio E_1/E_2 *versus* k for various parametric values of ω and for plane-strain conditions.

old crack-axis (O_1O_1-axis). If along this new path the crack propagates along the length O_1O_2, at the point O_2 the crack subtends an angle $|\vartheta_{\min,2} - \vartheta_{\min,1} + \omega|$ with the initial transverse crack-axis (Ox-axis). Because of the new position and orientation of the crack at the vicinity of its tip, the crack will propagate now along the direction O_2O_3 subtending a new angle $-\vartheta_{\min,3}$ with the previous crack-axis (O_1O_2-axis).

In this way the crack follows a zig-zag path and the angles subtended between

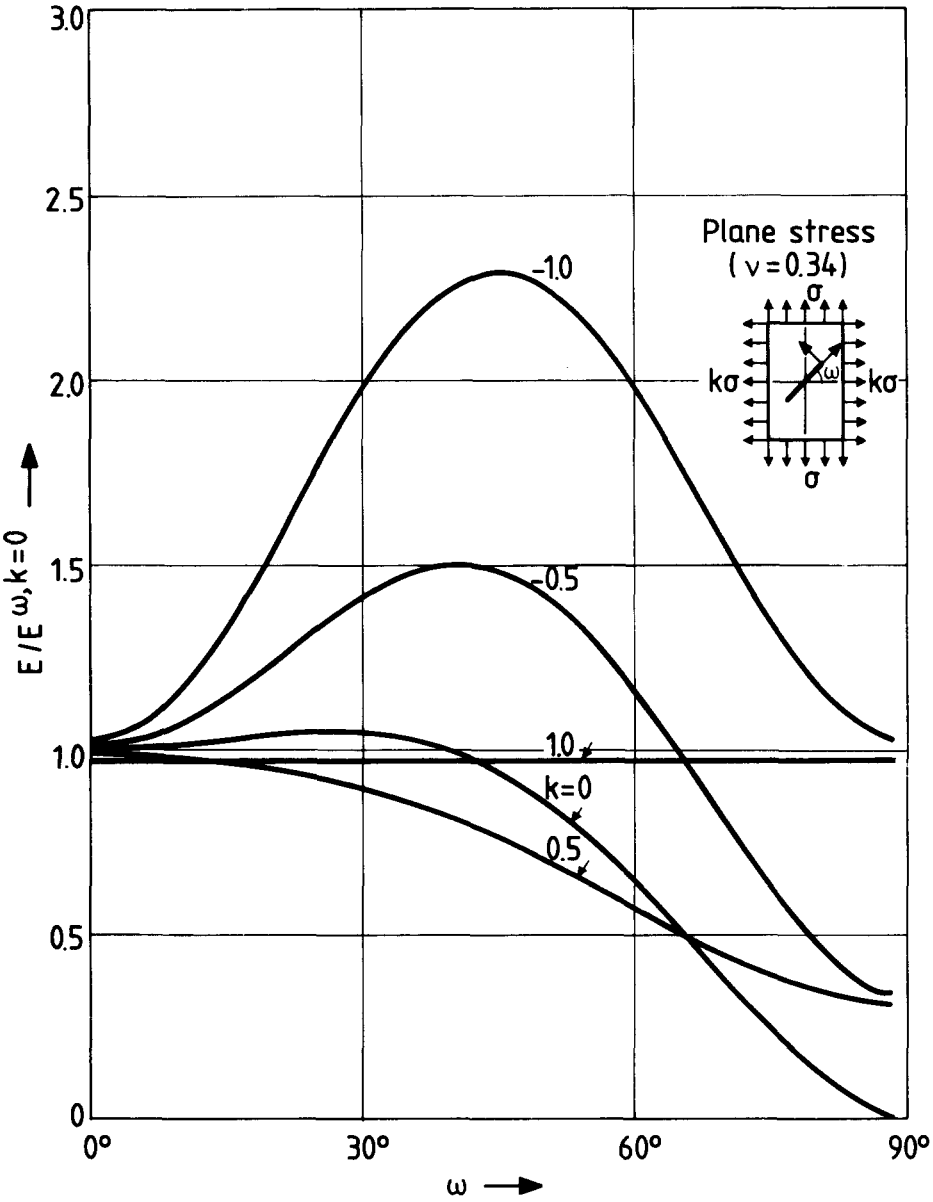

Figure 12a. Variation of the total area $E = (E_1 + E_2)$, normalized to the respective area for $\omega = 0$ and $k = 0$ (transverse crack for uniaxial tension, $K_{II} = 0$) *versus* ω, for various parametric values of k and for plane-stress conditions.

each small step with the transverse direction (Ox-axis) are given by (Fig. 14):

$$|\vartheta_{\min,1} - \omega| > |\vartheta_{\min,2} - \vartheta_{\min,1} + \omega| > |\vartheta_{\min,3} - \vartheta_{\min,2} + \vartheta_{\min,1} - \omega| > \\ > \ldots > |\vartheta_{\min,n} - \vartheta_{\min,(n-1)} + \cdots + (-1)^n \omega|, \quad n = 1, 2, 3, \ldots \infty \tag{28}$$

The zeroing of the slope of the crack after a number of steps indicates that the crack after a sufficient number of zig-zag kinks tends to a horizontal axis where only K_I is operative.

The assumption that the crack follows a zig-zag path is derived from the fact that the angles $-\vartheta_{\min,i}$ at every step remain always larger than the corresponding angle of

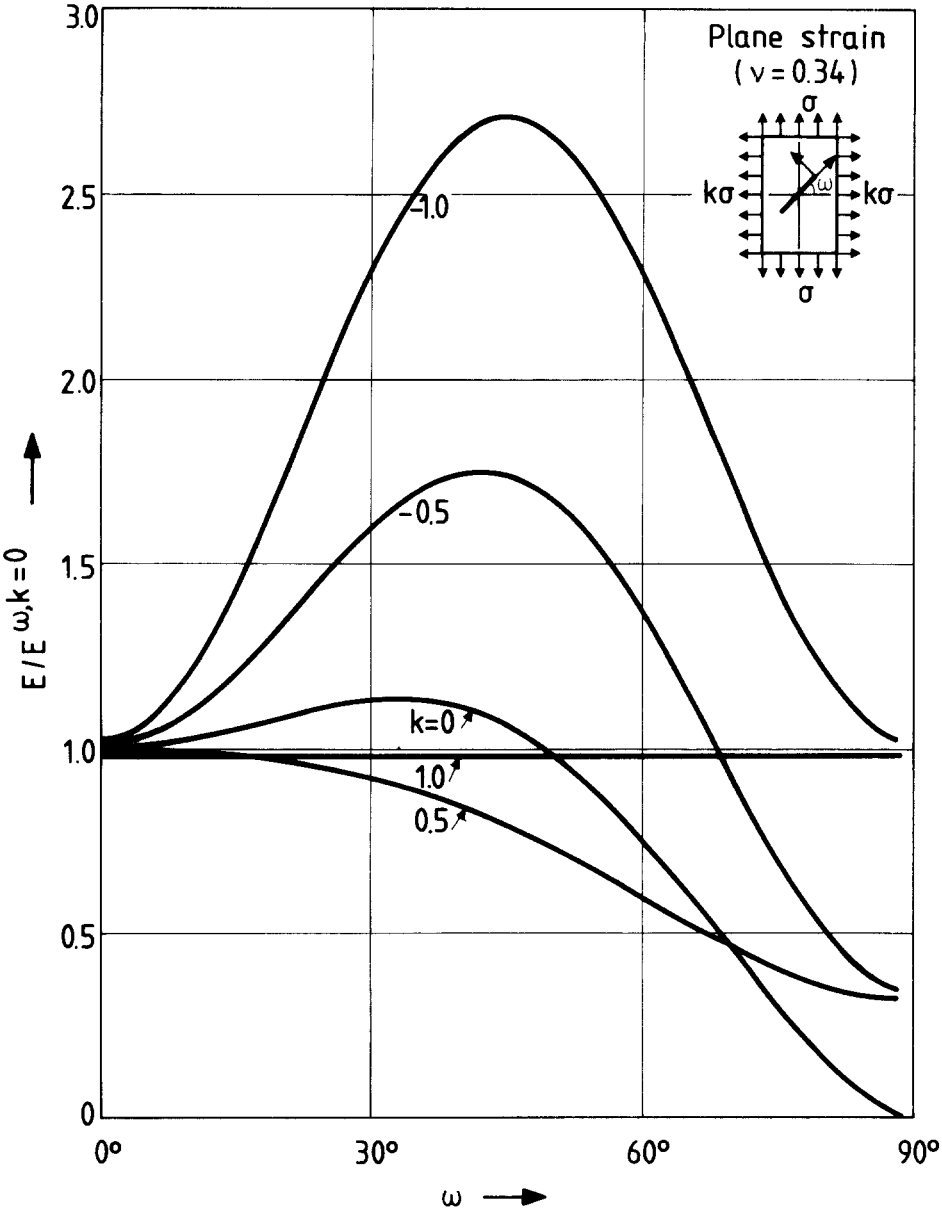

Figure 12b. Variation of the total area $E = (E_1 + E_2)$ normalized to the respective area for $\omega = 0$ and $k = 0$ (transverse crack for uniaxial tension, $K_{II} = 0$) *versus* ω, for various parametric values of k and for plane-strain conditions.

inclination of the crack at the previous step. This can readily be derived by observing Figs. 6(a, b) and 7(a, b). Thus, we have:

$$
\begin{aligned}
&|-\vartheta_{\min,1}| > |\omega| \\
&|-\vartheta_{\min,2}| > |\vartheta_{\min,1} - \omega| \\
&|-\vartheta_{\min,3}| > |\vartheta_{\min,2} - \vartheta_{\min,1} + \omega| \qquad (29) \\
&\ldots\ldots\ldots\ldots\ldots\ldots\ldots \\
&\ldots\ldots\ldots\ldots\ldots\ldots\ldots \\
&|\vartheta_{\min,n}| > |\vartheta_{\min,(n-1)} - \vartheta_{\min,(n-2)} \cdots + (-1)^{(n-1)}\omega|
\end{aligned}
$$

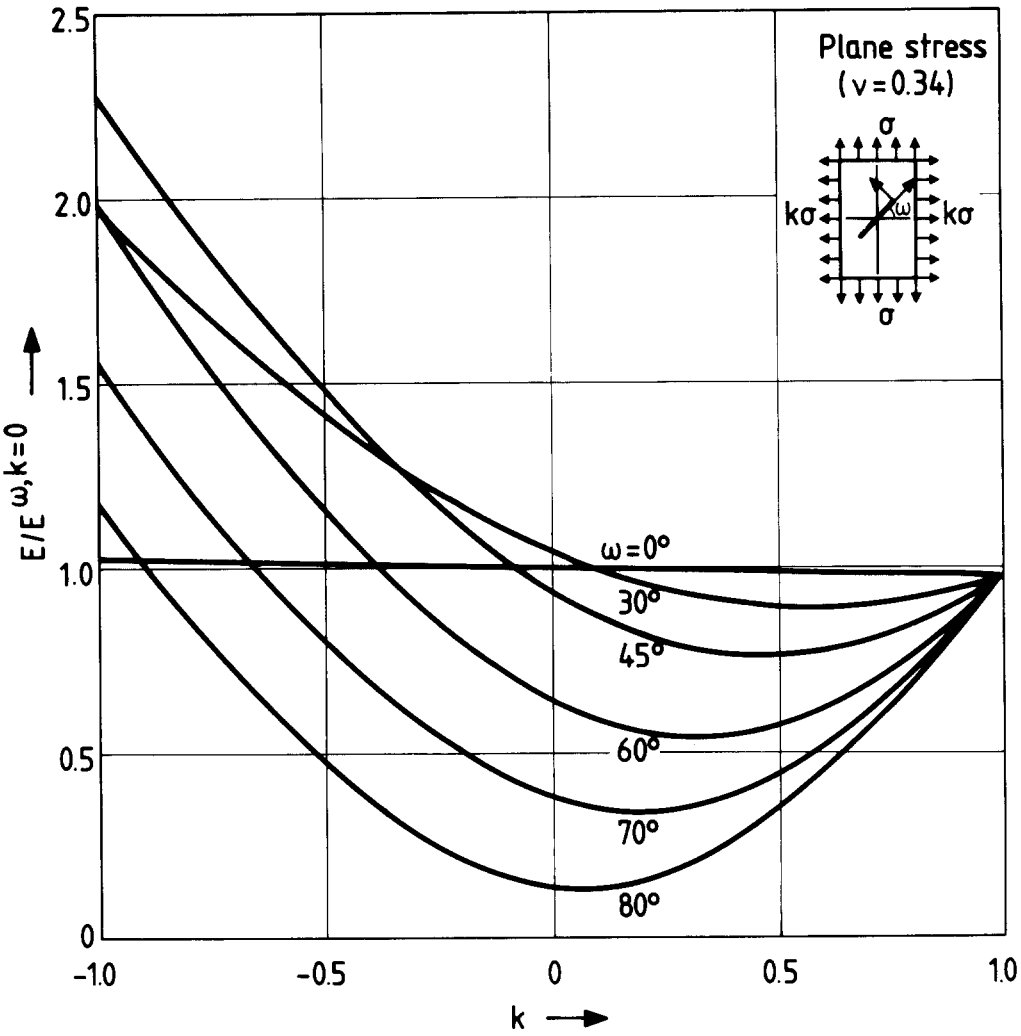

Figure 13a. Variation of the total area $E = (E_1 + E_2)$ normalized to the respective area for $\omega = 0$ and $k = 0$ (transverse crack for uniaxial tension, $K_{II} = 0$) *versus* k for various parametric values of ω and for plane-stress conditions.

Relations (29) are valid only for $\omega < 60°$ for $k = 0$. For $\omega = 60°$ the angle of orientation of ϑ_{min} equals the angle of the crack-axis, that is:

$$|-\vartheta_{min,n}| = |\vartheta_{min,(n-1)} - \vartheta_{min,(n-2)} + \cdots + (-1)^{(n-1)}\omega| \tag{30}$$

For the cases where relation (30) is valid the crack is propagated in a straight line along the transverse direction of the specimen.

Figure 15 presents various cases of crack propagations. Figs. 15a and b indicate the zig-zag direction for initial cracks subtending angles $\omega = 30°$ and $45°$ ($\mu = 0.58$ and 1.00 respectively) when the cracked plate is submitted to a uniaxial tension ($k = 0$). The zig-zag steps are clearly indicated and the angles subtended between them. Fig. 15c presents the case where relation (30) is valid in a plate with an initial-crack axis subtending an angle $\omega = 60°$ with the horizontal transverse axis of the specimen ($\mu = 1.73$, $k = 0$). According to this model the crack will propagate straight ahead in a transverse direction.

For cases where $\omega > 60°$ ($\mu > 1.73$) it may be observed that, for the first step of

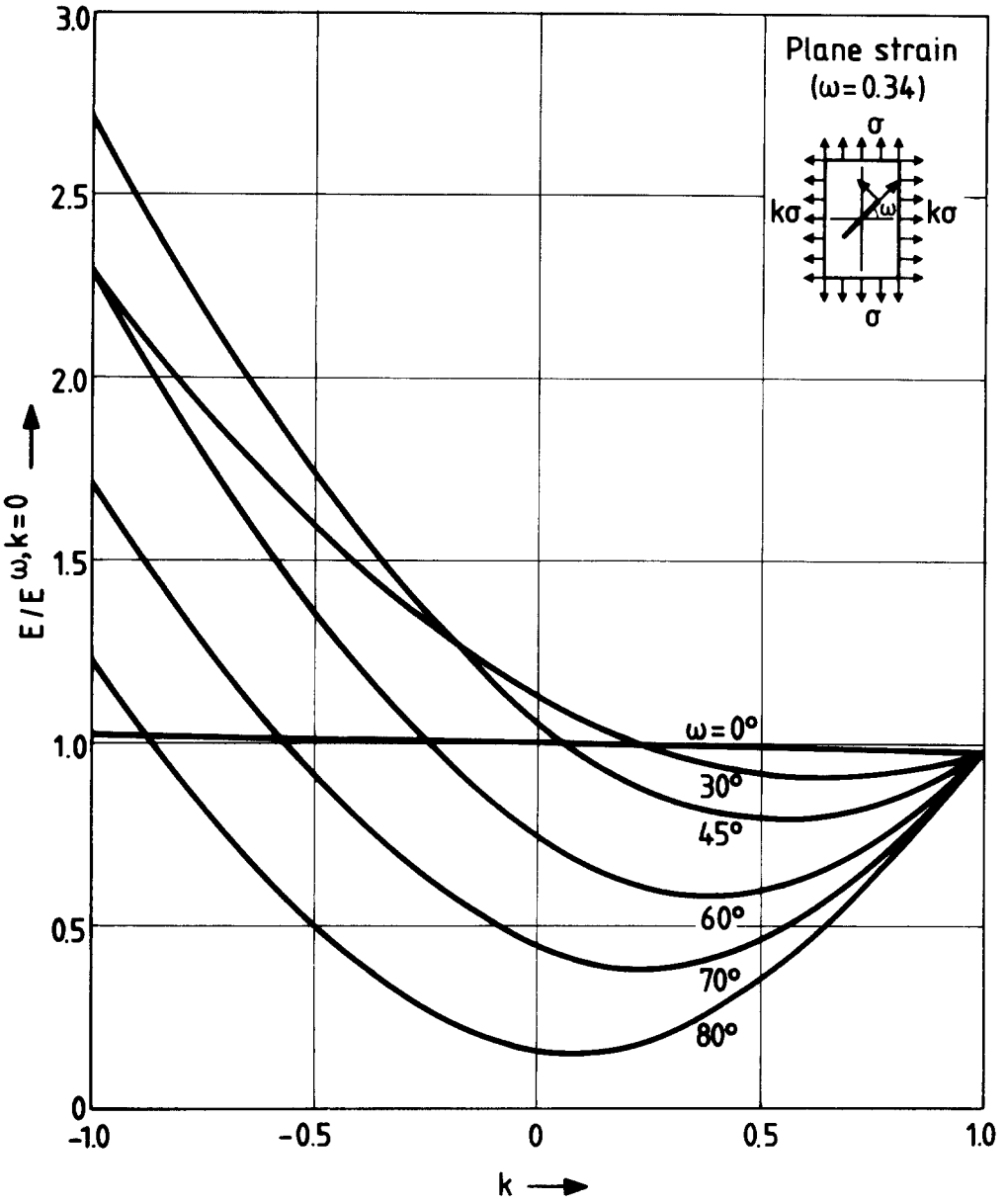

Figure 13b. Variation of the total area $E = (E_1 + E_2)$ normalized to the respective area for $\omega = 0$ and $k = 0$ (transverse crack for uniaxial tension, $K_{II} = 0$) *versus* k for various parametric values of ω and for plane-strain conditions.

the crack, the distribution of the elastic strain-energy around the singular core presents a minimum at an angle given by:

$$|-\vartheta_{\min,1}| < |\omega| \tag{31}$$

while the subsequent steps are obeying relations (29). In these cases the zig-zag procedure starts from the second step. A typical example is shown in Fig. 15d with a crack having $\omega = 80°$ ($\mu = 5.67$, $k = 0$).

All crack-paths in Fig. 15 were sketched for uniaxial tension ($k = 0$), they are

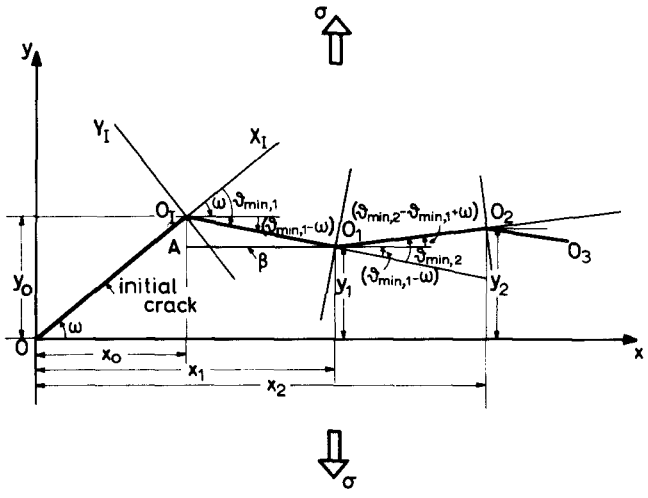

Figure 14. Model of a propagating crack corestructed according to the minimum strain-energy-density criterion.

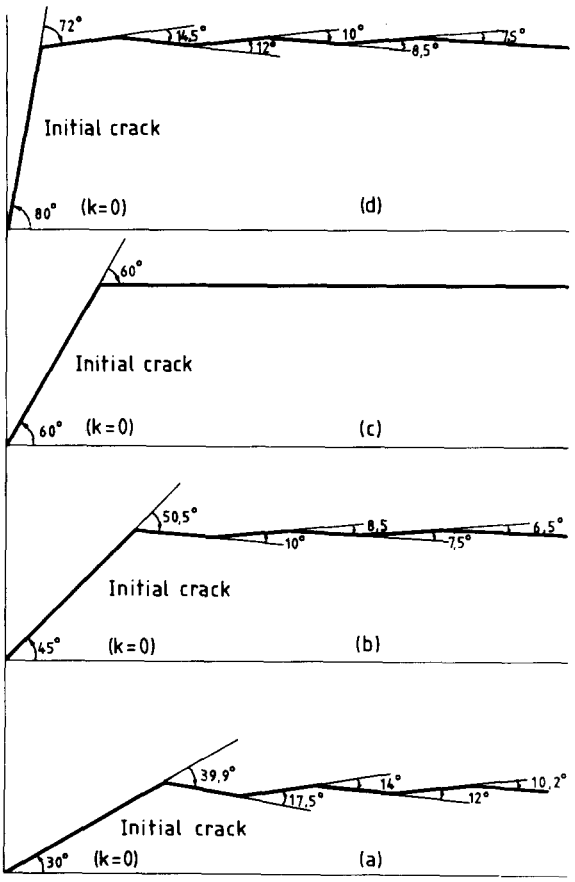

Figure 15. Various cases of crack propagations for plane-stress conditions and for $k = 0$ which correspond to a uniaxial tension (a) $\omega = 30°$ (b) $\omega = 45°$ (c) $\omega = 60°$ and (d) $\omega = 80°$.

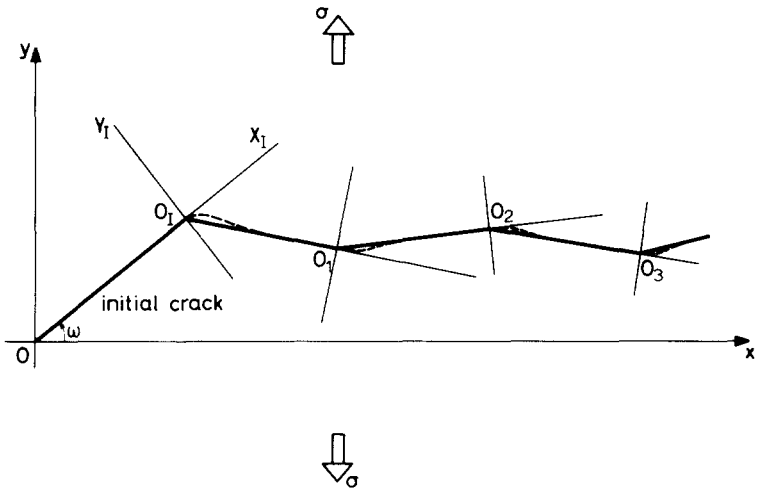

Figure 16. The influence of the singularities existing at the corners O_I, O_1, O_2, O_3 etc. of a zig-zag crack on the subsequent propagation of its branches.

based on the nomograms of Figs. 6a and 7a for plane-stress conditions, and the propagation steps assumed equal to each other and arbitrary.

In this model of the propagation of the crack we assumed that the crack is propagating by steps by a process of coalescence of voids created during fracture in front of the crack tip and at the vicinity of the crack. The length of these steps should be very small. According to Kfouri [17] the crack propagates by quantum steps,

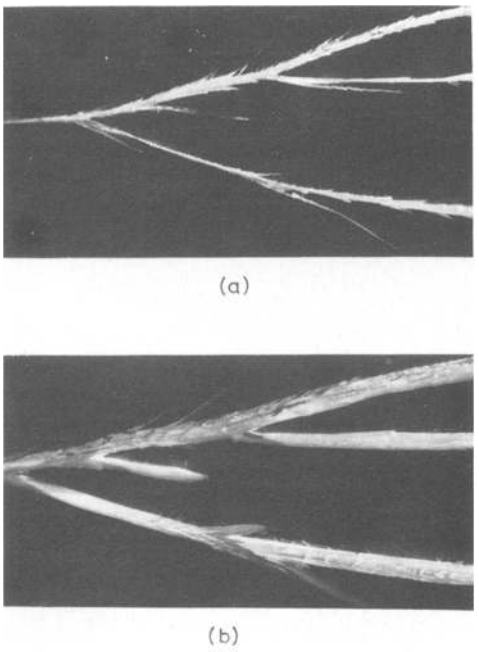

Figure 17. A multibranched crack developed in a polycarbonate thick specimen (thickness d = 0.010 m) where the phenomena of branching and rotation of the crack are clearly indicated. Fig.(a) shows the crack path in a normal incidence of observation, whereas Fig(b) in an oblique one thus yielding the shapes of branches through the thickness of the specimen.

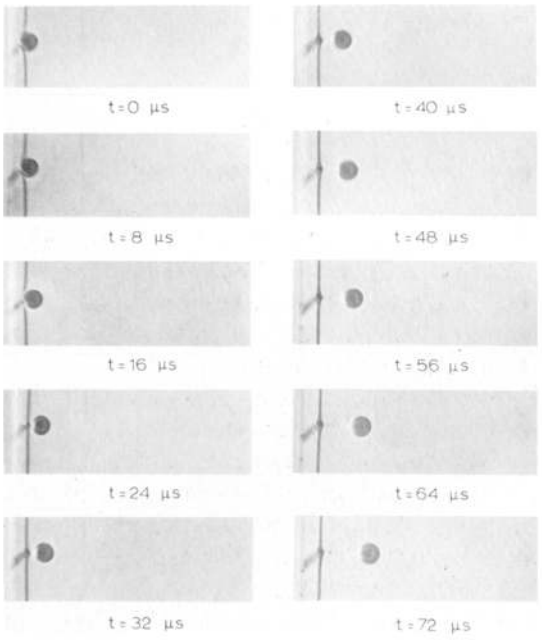

Figure 18. Mode of rotation of a subsequent kink evaluating from the corner of an oblique crack at an angle $\omega = 45°$ existing in a simple tension specimen made of plexiglas as indicated by the relative rotation of the caustics formed at the crack tip.

related to the energy per surface unit, necessary for the separation of the lips of the crack. This assumption seems reasonable and necessitates further tests.

From the definition of the path of the propagating crack a relation may be derived which may describe the mode of propagation of cracks.

If $x_0 = a \cos \omega$ and $y_0 = a \sin \omega$ are the coordinates of the tip O_1 of the initial crack of length a, then:

$$y_0 = x_0 \tan \omega$$

The coordinates of the tip O_1, which are denoted as x_1 and y_1, are given by:

$$y_1 = y_0 - (O_1A) = y_0 - (AO_1) \tan(|\vartheta_{\min,1}| - \omega)$$

or:

$$y_1 = x_0 \tan \omega + (x_1 - x_0) \tan(\omega - |\vartheta_{\min,1}|)$$

Proceeding in the same way for all intermediate crack tips we have the relation:

$$y_i = y_{(i-1)} + (x_i - x_{(i-1)}) \tan\left(\omega + \sum_{n=1}^{i} (-1)^n |\vartheta_{\min,n}|\right) \tag{32}$$

with $i = 1, 2, 3, \ldots \infty$ the number of the zig-zag steps in the crack propagation procedure.

In relation (32) the term $(x_i - x_{(i-1)}) = \beta$ is the projection of each propagation step on the transverse Ox-axis. Thus, the abscissa x_i of each crack-tip O_i corresponding to the step i is given by:

$$x_i = \beta + x_{(i-1)} \tag{33}$$

Relations (32) and (33) yield the coordinates of each crack tip O_i and through

them the crack path can be defined. Relation (32) may be written as:

$$y_i = a \sin \omega + \beta \sum_{\delta=1}^{i} \tan\left(\omega + \sum_{n=1}^{\delta} (-1)^n |\vartheta_{\min,n}|\right) \tag{34}$$

with $\delta = (1, 2, 3, \ldots, i)$ and $n = (1, 2, 3, \ldots, \delta)$.

Figure 19 presents the photographs of crack paths in plexiglas specimens submitted to uniaxial tension ($k = 0$). The initial artificial cracks were chosen to subtend angles with the horizontal Ox-axis of the specimen equal to $\omega = 45°$ (Fig. 19a) $\omega = 60°$ (Fig. 19b) and $\omega = 80°$ (Fig. 19c). It may be observed from the paths of the crack-axes that, in the first case with $\omega = 45°$, the crack is propagating with an angle $\vartheta_{\min,1}$ larger than the angle of initial inclination. In the second case with $\omega = 60°$ there is a straight and transverse propagation of the crack, whereas for $\omega = 80°$ $\vartheta_{\min,1} < \omega$. Thus, the experimentally obtained crack paths follow exactly the paths defined by the crack model based on the minimum elastic-strain-energy density principle.

The angular displacement of the steps following the initial crack which is not a natural crack, but an artificial crack created by a saw-cut, is not influenced by this fact. This becomes evident if one compares the natural cracks shown in Fig. 17, which, at the beginning of their creations, present this continuous bending of their axes and then stabilize to a certain angle. The behaviour of these branches emanating from the natural main crack is identical to the behavior of the crack kinks shown in Fig. 19 following artificial cracks. Moreover, there is also a coincidence of the behavior indicated in Fig. 18 with the behavior of natural cracks.

In Fig. 20 the particular values for the angles $\vartheta_{\min,1}$ corresponding to the first step of the crack propagation which coincide with the angles of inclination of the initial cracks were plotted versus the loading ratio k for either plane-stress, or plane-strain conditions in the cracked plate, as they have derived by applying the minimum elastic

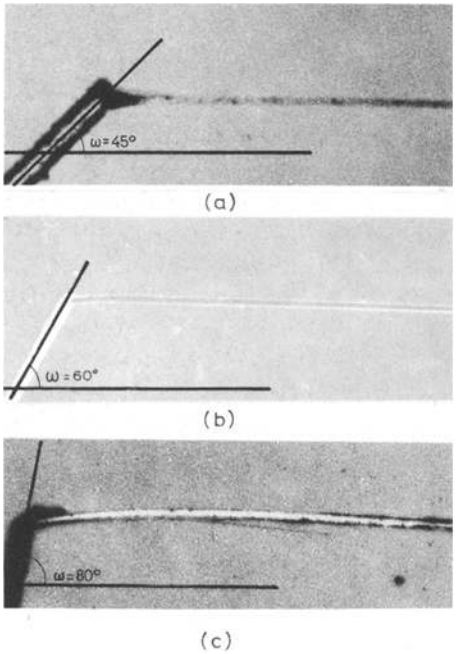

Figure 19. Crack propagation in an isotropic material (plexiglas) with different angles of inclination of the initial crack: (a) $\omega = 45°$ (b) $\omega = 60°$ (c) $\omega = 80°$ for $k = 0$ (uniaxial tension).

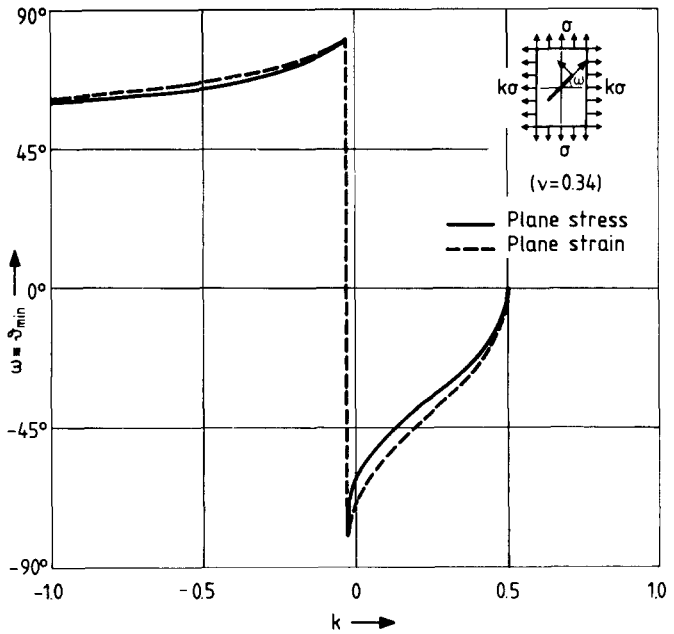

Figure 20. Variation of $\omega \equiv \vartheta_{min}$ *versus* k for plane-stress and plane-strain conditions.

strain energy principle. It may be observed from these plots that for uniaxial tension ($k = 0$) we have a straight transverse propagation of the crack (without any zig-zag) for an initial inclination of the stationary crack $\omega = 60°$ for plane stress and $\omega = 70°$ for plane-strain conditions. For biaxial equal tension at infinity ($k = 1$) a straight linear propagation can be achieved for $\omega = 0°$ for plane-stress and plane-strain conditions. Finally, for a tension-compression case ($k = -1$) the straight propagation appears for $\omega = 60°$ (plane-stress) and $\omega = 61°$ (plane-strain).

Acknowledgement

The research work contained in this paper is a part of the Doctor of Sciences thesis of the second author. The research programme was partly supported by funds of the Research Committee of the University and partly by the Hellenic Aluminium Co. The authors express their gratitude for this financial help.

REFERENCES

[1] G.C. Sih, *International Journal of Fracture* 10 No. 3 (1974) 305–321.
[2] G.C. Sih, *Journal of Engineering Fracture Mechanics* 5 (1973) 365–377.
[3] G.C. Sih, *Application of the Strain-Energy-Density Theory to Fundamental Fracture Problems*, Institute of Fracture and Solid Mechanics, Technical Report, Lehigh University (1972).
[4] G.C. Sih, Introductory Chapter in *Mechanics of Fracture* 1, Noordhoff (1972).
[5] J. Riedmüller, *Experimentelle Bestimmung der Energiedichteverteilung in der Nähe von Risspitzen bei überlagerter Normal- und Scherbeanspruchung*, Wissenschaftlicher Bericht, Institut für Festkörpermechanik der Fraunhofer-Gesellschaft e.v., Freiburg i. Br. (August 1975).
[6] P.S. Theocaris, *Applied Optics* 10 No. 10 (1971) 2240–2247.
[7] P.S. Theocaris and E. Gdoutos, *Journal of Applied Mechanics* (1972) 91–97.

[8] P.S. Theocaris and C.I. Razem, *International Journal of Mechanical Sciences* (1981) to be published.
[9] F. Erdogan and G.C. Sih, *ASME Journal of Basic Engineering* 85D (1963) 519–527.
[10] G.C. Sih, Introductory Chapter in *Mechanics of Fracture*, 2, Noordhoff (1975).
[11] A.A. Griffith, *Philosophical Transactions of the Royal Society* 221 Series A (1921) 163–198.
[12] A.A. Griffith, *The Theory of Rupture, Proceeding, First International Congress of Applied Mechanics*, Delft (1924) 55–63.
[13] J.G. Williams and P.D. Ewing, *International Journal of Fracture Mechanics* 8, No. 4 (1972) 441–446.
[14] N.I. Muskhelishvili, *Some Basic Problems of the Mathematical Theory of Elasticity*, 4th Edn. Noordhoff, Groningen (1963).
[15] J. Eftis and N. Subramonian, *Engineering Fracture Mechanics* 10 (1978) 43–67.
[16] P.S. Theocaris and G.A. Papadopoulos, *Materialprüfung* 22, No. 6 (1980) 246–253.
[17] A.P. Kfouri, *International Journal of Fracture* 15 No. 1 (1979) 23–29.
[18] P.S. Theocaris and E.E. Gdoutos, *Journal of Applied Mechanics* 18 No. 1 (1976) 64–68.
[19] G.J. Tsamasphyros et P.S. Theocaris, *Journal de mécanique* 15, No. 4 (1976) 615–630.

RÉSUMÉ

L'étude de la distribution de la densité d'énergie de déformation élastique à l'extrémité d'une fissure présente une intéret particulier pour comprendre le mécanisme de la rupture. Dans cette étude, on a développé une analyse théorique exhaustive de la distribution de la densité d'énergie de déformation élastique à l'extrémité d'une fissure dans le cas de fissures situées dans un milieu élastique isotrope déformé selon les models I et II. Cette étude a été complétée par une solution expérimentale de ce type de problème basée sur la méthode des caustiques réfléchies. Selon cette méthode, la distribuiton de la densité d'énergie de déformation élastique est évaluée le long d'une courbe fermée circulaire définissant un noyau singulier autour de l'extrémité de la fissure qui est influencé par la singularité à l'extrémité de la fissure, et dont le diamètre est tres petit et n'excède pas quelques millimètres. Par cette voie, la situation à la singularité de lextrémité de la fissure a été dépeinte directement sur base de la distribution de densité d'énergie. Des résultats intéressants concernant les facteurs qui influencent le mode de distribution d'énergie de déformation au voisinage de la fissure ainsi que du type de chemin de fissuration ont pu être dérivés.